Biophysical Journal
Article

Biophysical Society

Protein friction and filament bending facilitate contraction of disordered actomyosin networks

Alexander K. Y. Tam,[1,*] Alex Mogilner,[2] and Dietmar B. Oelz[1]
[1]School of Mathematics and Physics, The University of Queensland, St Lucia, Australia and [2]Courant Institute of Mathematical Sciences, New York University, New York, New York

ABSTRACT We use mathematical modeling and computation to investigate how protein friction facilitates contraction of disordered actomyosin networks. We simulate two-dimensional networks using an agent-based model, consisting of a system of force-balance equations for myosin motor proteins and semiflexible actin filaments. A major advantage of our approach is that it enables direct calculation of the network stress tensor, which provides a quantitative measure of contractility. Exploiting this, we use repeated simulations of disordered networks to confirm that both protein friction and actin filament bending are required for contraction. We then use simulations of elementary two-filament systems to show that filament bending flexibility can facilitate contraction on the microscopic scale. Finally, we show that actin filament turnover is necessary to sustain contraction and prevent filament aggregation. Simulations with and without turnover also exhibit contractile pulses. However, these pulses are aperiodic, suggesting that periodic pulsation can only arise because of additional regulatory mechanisms or more complex mechanical behavior.

SIGNIFICANCE Actomyosin contraction is a vital process in cell movement and division. We introduce an energy minimization framework for modeling actomyosin networks that enables direct calculation of forces and stress. Using simulations, we show that protein friction and actin filament bending facilitate network-scale contraction. On the microscopic scale, we define a heuristic index that explains bending-induced contraction in terms of motor position and mutual filament angle. On the network scale, we show that turnover prevents pattern formation and enables persistent, aperiodic contraction.

INTRODUCTION

The mechanics of actomyosin networks govern essential cellular processes, including muscle contraction (1), cell division (2), and cell motility (3). Assemblies of actin and myosin exhibit diverse structural organization. In muscles, actin filaments are aligned in parallel to form sarcomeres, in which myosin-II motor proteins generate force in accordance with the sliding filament theory (1). Alternatively, actin filaments form a disordered two-dimensional meshwork in the cell cortex, located below the membrane of living cells. These filaments are cross-linked by myosin motors, which exert forces that give rise to cortical tension and flow (4). This cortex deformation subsequently determines cellular morphology and locomotion. Understanding the mechanisms by which myosin motors generate local forces is challenging and can be investigated using mathematical modeling and computation.

The sliding filament mechanism provides a starting point for investigating contraction in disordered networks. Myosin motors attached to pairs of parallel actin filaments can generate either contraction or expansion, depending on filament orientation. A motor protein bound to a pair of filaments with barbed ends facing outwards will generate local contraction, as shown in Fig. 1*A*. Conversely, the filaments generate expansion if the pointed ends face outwards (Fig. 1*B*). However, this sliding filament mechanism alone cannot explain net contraction in disordered networks, in which filaments can cross at arbitrary angles and in either configuration with equal probability. In these networks, there must be additional symmetry-breaking mechanisms that favor contraction over expansion.

Candidate mechanisms for generating contraction in disordered networks fall into the broad categories of structural and force asymmetries. Structural asymmetries break the random alignment of actin and myosin, enabling

Submitted March 4, 2021, and accepted for publication August 6, 2021.
*Correspondence: alex.tam@uq.edu.au
Editor: Timo Betz.
https://doi.org/10.1016/j.bpj.2021.08.012

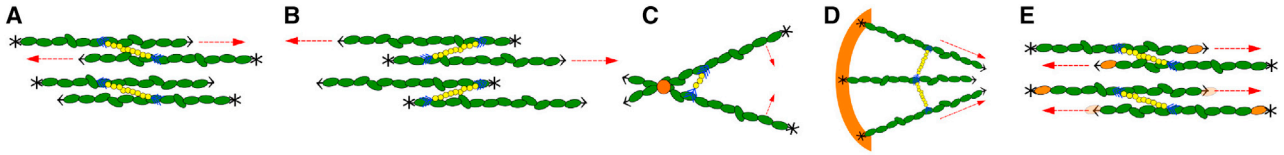

FIGURE 1 Schematic representations of (*A*) contraction via the sliding filament mechanism, (*B*) expansion via the sliding filament mechanism, (*C*) filament zippering, (*D*) filament anchoring, and (*E*) actin treadmilling. Asterisks indicate filament barbed (plus) ends, and arrow heads indicate pointed (minus) ends. Dashed arrows represent direction of filament movement. To see this figure in color, go online.

contractile configurations to emerge more often than expansive ones. Force asymmetries arise if filaments behave differently under tension and compression, enabling contraction more readily than expansion. In cells, mechanisms of contraction can be redundant and act as fail-safes in case network components are absent or lose function (5–7). Many contractile mechanisms have been proposed and investigated for this reason.

Several hypotheses exist for generating structural asymmetries in two-dimensional networks. One example is a zippering mechanism, whereby a motor with nonzero length is displaced ahead of the intersection between two filaments (see Fig. 1*C*). Motor movement toward the plus ends then pulls the filaments inwards, generating contraction (8–10). Theoretical work by Lenz (9) showed that zippering can generate net contraction in disordered networks but is unlikely to occur in practice. Another possible structural asymmetry is based on the observation that some filaments grow with barbed ends anchored to the cell membrane (5,6) (see Fig. 1*D*). Contraction can then occur via the sliding filament mechanism because the anchored filaments are in a contractile alignment. However, a drawback of this hypothesis is that only a small fraction of filaments in the cortex are anchored, such that nonanchored filaments are thought to play a major role in contractility (6). A third hypothesized structural asymmetry for generating contraction is actin treadmilling, which involves simultaneous filament depolymerization at minus ends and polymerization at plus ends (11). This enables contractile structures to persist as barbed ends are pulled inwards, generating a structural asymmetry (see Fig. 1*E*). Oelz, Rubinstein, and Mogilner (12) showed that treadmilling gives rise to network-scale contraction in one-dimensional ring-like geometry. Previous theoretical work has also shown that myosin motors lingering at filament barbed ends instead of unbinding can generate contraction (9,13,14). However, although this behavior has been observed in experiments, it is not known whether it occurs in nonmuscle cells (15).

In contrast to these structural asymmetries, many studies consider a mechanism whereby filaments buckle, and possibly sever (16), under longitudinal compression. Because filaments can sustain longitudinal tension without buckling, this gives rise to asymmetric force propagation that favors contraction. Buckling has been illustrated in vitro (16) as well as theoretically (17) and occurs if filament length exceeds a threshold length. Another possible force asymmetry arises when filaments bend elastically in response to transverse forces (9). Filament bending is likely to be relevant in cellular actomyosin, because the forces exerted by myosin motors are large enough to bend filaments with lengths below 1 μm (16), which is the approximate filament length (18). However, the forces required to initiate bending are $\sim$1000 times smaller than those required to rupture filaments (19). Therefore, filament bending without buckling might also play a role in contraction.

Mathematical modeling has facilitated advancements in understanding actomyosin contraction. One phenomenological approach is to treat the actomyosin network as an active gel continuum (13,20). In these models, filament and motor positions are expressed in terms of continuous density fields. Although these models can effectively predict pattern formation in actomyosin networks (21), many recent models focus on developing accurate microscopic descriptions of network components. Because we are interested in whether actin filament bending can induce contraction on both the microscopic and network scales, we focus on coarse-grained agent-based models. These models use simplified representations of individual network components and track how they evolve over time. Agent-based models enable detailed description of the mechanics on a microscopic scale and can subsequently be used to derive accurate continuum models (22).

Many agent-based models for the cytoskeleton exist, including publicly available software Cytosim (23), AFINES (24), and MEDYAN (25). These, and many other authors (7,26–29), use modified Brownian dynamics to simulate actomyosin networks. Under this approach, actin filaments move according to an overdamped Langevin-like equation for the balance of forces between network components (7,23–29). Within this framework, many authors have recognized the importance of filament bending forces to contractility (7,14,24,30–33). A common approach is to focus on filament buckling (17,24,32,34,35) as a mechanism of contraction. This represents an extreme case of force asymmetry generated by deformable filaments. Using a one-filament worm-like chain model, Lenz (9) showed that motor-induced filament bending is more effective than filament buckling at facilitating contraction and is relevant for typical experimental parameters. However, further quantitative analysis of this bending force asymmetry in filament networks is required.

Protein friction can be represented as effective viscous drag that acts pointwise at the binding site of a motor or cross-linker or at the point of contact between filaments (36). Using a one-dimensional model, Oelz, Rubinstein, and Mogilner (12) showed that a combination of actin treadmilling and drag distributed along filament pairs that overlap can contract a ring-like network of rigid filaments. In two dimensions, protein friction manifests as pointwise drag at filament intersections (37,38). McFadden et al. (38) showed that pointwise drag and bending force asymmetry facilitate contraction. These models with protein friction draw parallels between pointwise drag and cross-linkers (37,38). However, this implies that cross-linkers are either short and abundant or turn over rapidly. The possibility of using pointwise drag to represent solid friction between filaments remains largely unexplored, and additional work is required to determine how this affects network contraction.

To address these research gaps, we develop a mathematical model for semiflexible actin filaments and myosin motors to investigate how protein friction affects contractility. A promising simulation approach was developed by Dasanayake, Michalski, and Carlsson (39) and Hiraiwa and Salbreux (10), in which the network configuration is given by the minimizer of a potential energy functional. However, these studies considered the evolution of random networks to a steady state and neglected longer-time evolution of the network. In developing our model, we extend this approach to fully time-dependent simulations.

MATERIALS AND METHODS

Mathematical model

We develop an agent-based model to simulate two-dimensional disordered networks. The network contains semiflexible actin filaments, which we represent as finite-length curves in two-dimensional space. We represent myosin motors as dumbbells that behave as linear springs with equilibrium length zero such that they attach to filament pairs at intersections. We assume that myosin motors detach immediately if they reach a filament plus end and otherwise model force-dependent random detachment according to Bell's law (40). Movement of unattached motors is not modeled explicitly. Instead, we assume that a new motor immediately attaches at a random filament intersection when an unbinding event occurs. Although this is not representative of real networks, it enforces that the density of active motors remains constant. This ensures variation in the number of motors cannot influence the results. We then simulate network evolution by solving for the positions of filament nodes and myosin motors on a square domain with periodic boundary conditions.

Components in cytoskeletal networks undergo continuous turnover (33,41–43). This refers to the exchange of filaments, motors, and cross-linkers between the network and cytoplasm (10). Turnover can occur when filaments sever (16) or undergo treadmilling (12,44,45), which depends on motor (16) and cross-linker activity (35). We explicitly model actin turnover by removing filaments (and any attached motors) at random with a constant rate (10,38). When a filament is removed, we immediately replace it with a new one at a random position to maintain constant filament density. This represents a simple model for actin turnover, just as our treatment of myosin unbinding represents a simple model for motor turnover.

Protein friction is another mechanical feature that might influence network contractility (36,46). It can arise from binding and unbinding interactions between filaments and motors (46) or filaments and cross-linkers (47) or from solid friction between filament pairs in contact (48) (see Figure 1 *C*). Contact frictional forces are larger than hydrodynamic friction between filaments and the cytoplasm (47,48) and have comparable magnitude to forces exerted by myosin motors (48). In our model, we apply viscous drag at intersections between actin filaments to model protein friction originating from either cross-linking or filament contact (37,38). We assume that the presence of a myosin motor prevents protein friction via cross-linking or filament contact, and do not apply pointwise drag between filament pairs connected to the same motor. Our model then enables investigation of whether protein friction, in conjunction with actin filament bending, gives rise to contraction.

We write the core model as a system of force-balance equations, which contains all mechanical features included in the model. In abstract terms, the system of equations is

$$\mathbf{0} = \boldsymbol{F}_{a,\mathrm{drag}} - \delta E_{a,\mathrm{bend}} - \delta E_{a,\mathrm{spring}} + \boldsymbol{F}_{a,\mathrm{pf}} - \delta E_{m,\mathrm{spring}} + \boldsymbol{F}_{m,a}. \tag{1}$$

Actin filaments contribute to the force balance via viscous drag, bending, stretching, and protein friction. Viscous friction penalizes relative motion between actin filaments and the background medium, giving rise to drag forces $\boldsymbol{F}_{a,\mathrm{drag}}$. We account for filament bending via the variation of $E_{a,\mathrm{bend}}$, which sums the elastic potential energy along the extent of each filament. The contribution of longitudinal spring forces, $E_{a,\mathrm{spring}}$, follows Hooke's law with spring constant k_a. Because actin filaments are effectively inextensible (49), we assume that k_a is large. The symbol $\boldsymbol{F}_{a,\mathrm{pf}}$ represents pointwise drag due to protein friction, which opposes the relative motion of filament intersections. We also investigated the effect of including random filament motion due to thermal forces. These have only a small impact on stress and filament aggregation, so we neglect thermal forces in Eq. 1. Further details on their effects are provided in the Supporting materials and methods.

The system (Eq. 1) also contains two contributions relevant to myosin motors. Like for actin filaments, $E_{m,\mathrm{spring}}$ is the energy associated with longitudinal spring forces. These forces are governed by Hooke's law with the spring constant k_m, which we assume large to model the short length of myosin motors compared to actin filaments. For actin-myosin interactions, we adopt a linear force-velocity relation for myosin motors, written as $\boldsymbol{F}_{m,a}$. Under this assumption, unloaded motors move at the velocity V_m, and motors cannot move if force exceeds the stall force, F_s.

Numerical method and stress calculation

In each simulation, we represent actin filaments as chains of nodes, with adjacent nodes connected by straight line segments. We initialize filaments as straight entities with random center positions and orientations such that all nodes on the same filament are equidistant. Given the initial filament network, we place myosin motors at random intersections between filaments such that each intersection accommodates a maximum of one motor. To evolve the network, at each time step we construct and minimize the energy functional

$$E_{\mathrm{net}} := E_{a,\mathrm{drag}} + E_{a,\mathrm{bend}} + E_{a,\mathrm{spring}} + E_{a,\mathrm{pf}} + E_{m,\mathrm{spring}} + E_{m,a}. \tag{2}$$

This functional includes pseudoenergy terms $E_{a,\mathrm{drag}}$, $E_{a,\mathrm{pf}}$, and $E_{m,a}$, whose variations correspond to finite difference approximations of the force terms $\boldsymbol{F}_{a,\mathrm{drag}}$, $\boldsymbol{F}_{a,\mathrm{pf}}$, and $\boldsymbol{F}_{m,\mathrm{a}}$, which cannot be interpreted as variations of potential energy. Further details and mathematical descriptions of the energy terms in Eq. 2 are provided in the Supporting materials and methods.

Each time step, we use the limited-memory Broyden-Fletcher-Goldfarb-Shanno method to minimize Eq. 2 with respect to the positions of filament nodes and myosin motors. We perform this optimization using the Optim.jl (50) package in JULIA, using automatic differentiation (ForwardDiff.jl) to evaluate the gradient. Our energy minimization method is time implicit,

which enables comparatively large time steps without loss of numerical stability. One drawback is that large time steps enable only coarse simulation of filament turnover and motor unbinding. Also, our implementation using automatic differentiation is typically slower than explicit methods.

A key advantage of our energy minimization numerical method is that it enables direct computation of the forces on the domain boundary required to prevent uniform elongation and shear deformations. These forces aggregate the contributions of each filament and motor in the network and thus provide a measure of contractility. We compute these forces, $\boldsymbol{F}_x$ and $\boldsymbol{F}_y$, by adding extra terms to the energy functional and defining the total energy

$$E_{\text{total}} := E_{\text{net}} + \boldsymbol{F}_x \cdot \boldsymbol{L}_x + \boldsymbol{F}_y \cdot \boldsymbol{L}_y, \tag{3}$$

where $\boldsymbol{L}_x = (L_{xx}, L_{xy})$ and $\boldsymbol{L}_y = (L_{yx}, L_{yy})$ are vectors representing two edges of the domain. The vectors $\boldsymbol{F}_x = (F_{xx}, F_{xy})$ and $\boldsymbol{F}_y = (F_{yx}, F_{yy})$, illustrated in Fig. 2, contain the normal and shear forces acting on the domain boundaries.

In practice, we simulate the model on a two-dimensional domain of fixed geometry, keeping the vectors $\boldsymbol{L}_x$ and $\boldsymbol{L}_y$ constant. Minimizing Eq. 2 is then equivalent to minimizing Eq. 3, where the normal and shear force components are Lagrange multipliers that constrain the domain to constant size and shape. In numerical simulations, we solve the model using Eq. 2, then compute $\boldsymbol{F}_x = -\partial_{\boldsymbol{L}_x} E_{\text{net}}$ and $\boldsymbol{F}_y = -\partial_{\boldsymbol{L}_y} E_{\text{net}}$ using automatic differentiation. After calculating $\boldsymbol{F}_x$ and $\boldsymbol{F}_y$, we combine the force components to compute the two-dimensional plane stress tensor,

$$\boldsymbol{\sigma} = \begin{bmatrix} F_{xx}/L_{yy} & F_{xy}/L_{yy} \\ F_{yx}/L_{xx} & F_{yy}/L_{xx} \end{bmatrix}. \tag{4}$$

This describes the state of plane stress in the network at any time step. Although in-plane shear can produce nonzero out-of-plane normal stress (51,52), we neglect these in our description. To obtain a measure of contractility in a simulation, we define the bulk stress and time-averaged bulk stress

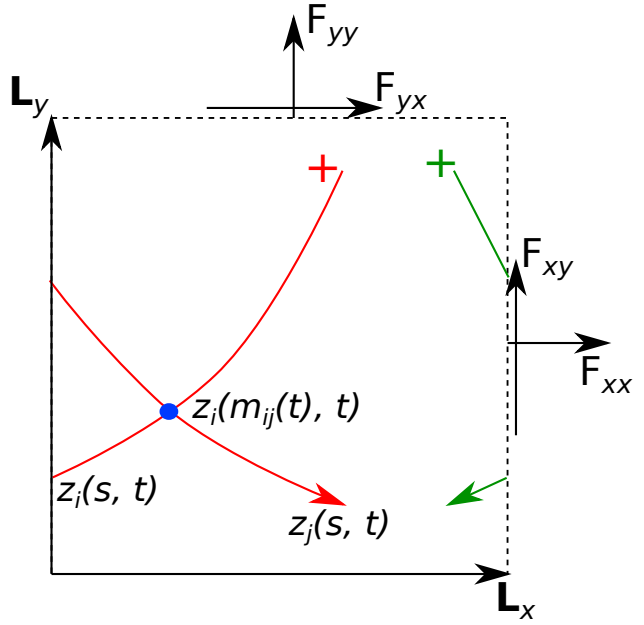

FIGURE 2 Schematic diagram of the periodic domain, two actin filaments, and a myosin motor. The vectors $\boldsymbol{z}_i(s, t) \in \mathbb{R}^2$ denote filament positions, parameterized by the arc length s. The variable $m_{ij}(t)$ is the position of the motor. To see this figure in color, go online.

$$\sigma = \frac{1}{2}\text{tr}(\boldsymbol{\sigma}) \quad \text{and} \quad \overline{\sigma} = \frac{1}{T}\int_0^T \sigma \, \mathrm{d}t, \tag{5}$$

respectively, where T is the time over which the simulation runs and $\text{tr}(\boldsymbol{\sigma})$ is the trace of the stress tensor, which is invariant to coordinate rotations. The trace is also equal to the sum of the eigenvalues of $\boldsymbol{\sigma}$, and the associated eigenvectors indicate the principal stress directions. By convention, negative $\overline{\sigma}$ indicates contraction, and positive $\overline{\sigma}$ indicates expansion. Our method of quantifying network stress enables addition or removal of features from the energy functional without changing the method of computing the forces. This flexibility is another advantage of our approach. In addition, our framework enables explicit simulation of domain deformation by treating $\boldsymbol{F}_x$ and $\boldsymbol{F}_y$ as applied external forces instead of Lagrange multipliers and $\boldsymbol{L}_x$ and $\boldsymbol{L}_y$ as degrees of freedom. Contractile networks would then cause $|\boldsymbol{L}_x|$ and $|\boldsymbol{L}_y|$ to decrease, and expansive networks would cause $|\boldsymbol{L}_x|$ and $|\boldsymbol{L}_y|$ to increase.

RESULTS AND DISCUSSION

We use numerical simulations of our mathematical model to investigate how filament bending and protein friction affect contractility. In general, we simulate actomyosin networks using a default set of biophysically realistic parameters obtained from literature (18,27,42,44,48,53–67). The complete list of parameter values and details on their estimation are provided in the Supporting materials and methods. We outline the main simulation results under subsequent headings.

Actin filament bending facilitates network contraction

To investigate actin filament bending as a contractile mechanism, we compared 25 simulations of semiflexible filaments with 25 simulations of rigid, straight filaments. In each simulation, we simulated 50 filaments and 10 motors in a domain of width 2.5 μm and ran simulations until $T = 60$ s, with a time step size of $\Delta t = 0.05$ s. This is sufficient to obtain results independent of the domain width and time step size (see Supporting materials and methods). We then compared the time-averaged bulk stresses (Eq. 5) and these reveal that bending is essential for contraction. As Fig. 3*A* shows, the network contracted in each simulation with semiflexible filaments (mean $\overline{\sigma} = -0.072$ pN μm^{-1}) but always expanded with rigid filaments (mean $\overline{\sigma} = 0.161$ pN μm^{-1}). With rigid filaments, we observe net expansion because motor movement biases mean motor position toward filament plus ends. In subsequent results (see Fig. 4), we will show this to be an expansive configuration. However, filament bending counteracts this tendency to expand, facilitating systematic bias to contraction.

We hypothesize that the magnitude of contraction depends on the extent of filament bending in the network. To investigate this, at each time step in the simulations we compute the local curvature

$$\kappa(s) = \sqrt{x''(s)^2 + y''(s)^2} \tag{6}$$

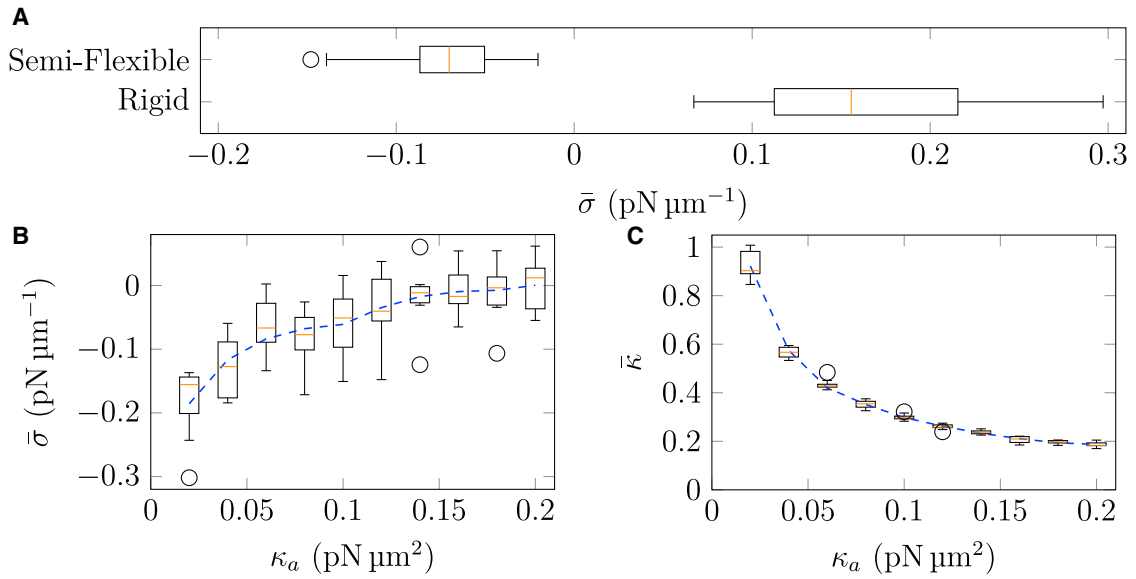

FIGURE 3 (*A*) Box plots comparing mean $\bar{\sigma}$ in 25 semiflexible networks and 25 rigid networks. (*B* and *C*) The effect of flexural rigidity, κ_a, on (*B*) $\bar{\sigma}$ and (*C*) $\bar{\kappa}$. Boxplots represent data from 10 simulations with a given parameter, and the dashed curve represents mean data smoothed with a Savitsky-Golay filter. To see this figure in color, go online.

at each filament node. To obtain a measure of total curvature for one filament, we use the trapezoidal rule to integrate the curvature along the filament. We quantify the extent of filament bending in the network by averaging the integrated curvature over all filaments and time, defining

$$\bar{\kappa} = \frac{1}{T}\frac{1}{N_a}\sum_{i=1}^{N_a}\int_0^T \int_0^{L_i} \kappa(s)\, \mathrm{d}s\, \mathrm{d}t. \tag{7}$$

In the remainder of this manuscript, bar notation will represent quantities similarly averaged over filaments and time.

Because the flexural rigidity describes the resistance of a filament to bending, we varied κ_a and investigated its effect on stress production. For each value of κ_a tested, we ran 10 random simulations and computed $\bar{\sigma}$. Box plots of network bulk stress presented in Fig. 3*B* show that decreasing κ_a increases contractility. This is expected because decreased values of κ_a correspond to decreased resistance to filament bending. As Fig. 3*C* shows, the increase in contractile stress that occurs with decreasing κ_a corresponds to increased filament curvature. This accords with the hypothesis that filament bending gives rise to force asymmetry and subsequently contraction. Furthermore, the flexural rigidity for actin filaments, $\kappa_a = 0.073$ pN μm^2 (55), lies within the region for which we expect contraction. Actin filament bending is thus a plausible mechanism of contraction in biological cells.

Bending facilitates net contraction on the microscopic scale

To better understand the microscopic mechanisms of contraction, we simulate systems of two actin filaments with an attached myosin motor. Our objective is to determine whether the force asymmetry occurs in this simple structure or whether contraction relies on network-scale interactions. In two-filament simulations, we use $\lambda_a = 10$ pN μm^{-2} s, which is larger than the value $\lambda_a = 0.05$ pN μm^{-2} s used in network simulations. This is because we assume the two-filament structure is embedded in a dense, homogeneous background network. When a single fiber is immersed in such a network, protein friction manifests itself as drag acting uniformly along the entire filament length. The larger value of λ_a then replaces protein friction at filament intersections, which cannot occur in the two-filament simulations because the motor occupies the only intersection.

We initialize the two filaments in a square domain and characterize their positions by the angle $\theta \in [0, \pi]$, which is the angle between the two filaments measured at their intersection point. The relative motor positions are denoted by m_1 and m_2 such that $m_i \in [0, L_i]$ for $i = 1, 2$ measures the distance of the motor binding site from the minus end of filament i. We hypothesize that the extent of expansion or contraction of the two-filament structure depends on θ, m_1, and m_2. As the motor slides the filaments, it pulls filament branches between the motor and plus ends together, generating contraction. Simultaneously, it pushes filament branches between the motor and minus ends apart, generating expansion. Furthermore, the filaments will move the most if they are antiparallel, or $\theta = \pi$. Conversely, when filaments are parallel ($\theta = 0$), the motor will traverse the filaments without generating relative motion.

Fig. 4, *A–J* illustrate two-filament simulations for both rigid and semiflexible filaments. In the upper row (Fig. 4, *A–E*), the rigid filaments evolve symmetrically. As the

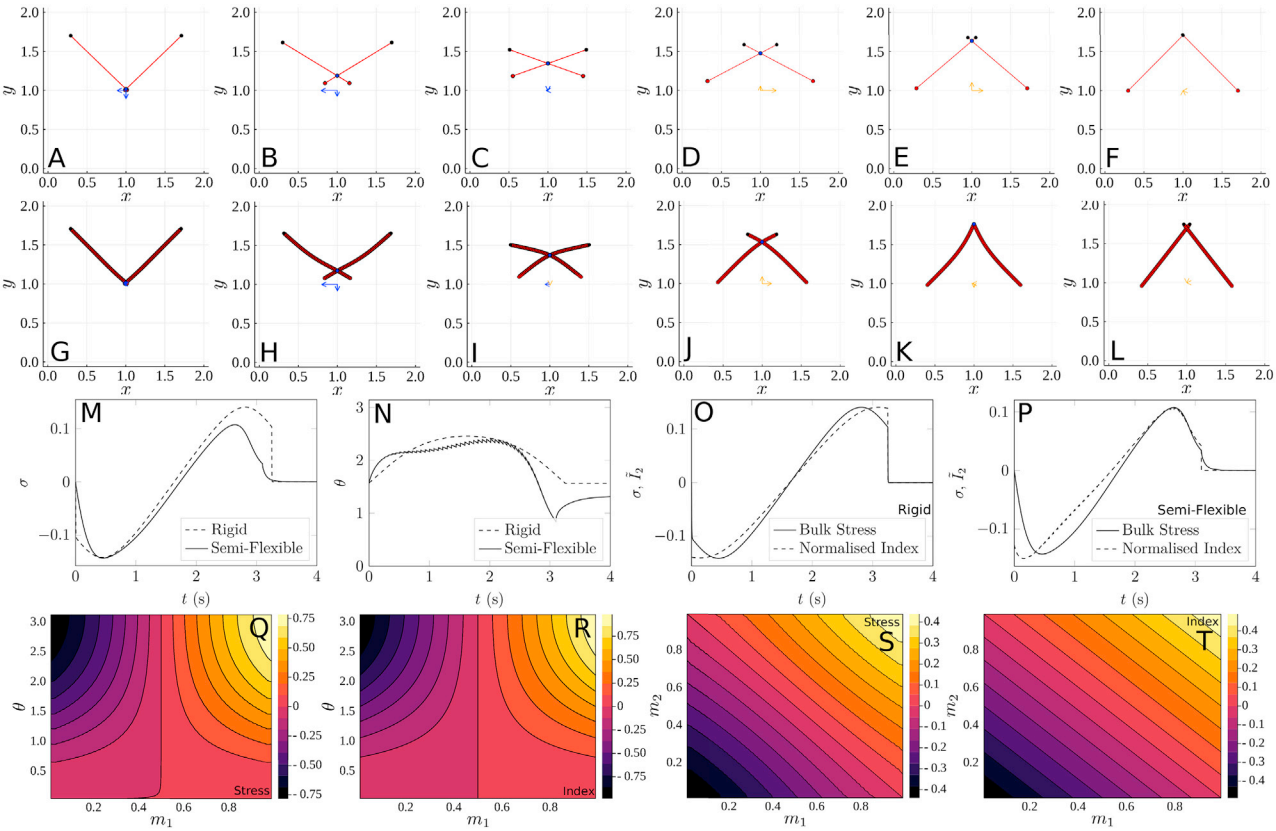

FIGURE 4 (*A–F*) Two-filament simulations with initial motor positions $m_1 = m_2 = 0$ and $\theta = \pi/2$. (*A–F*) Rigid actin filaments. (*G–L*) Semiflexible filaments. Results are presented (*left* to *right*) at $t \in \{0.04, 0.5, 1.55, 2.59, 3.09, 4\}$ s. Arrows centered at (1, 1) indicate the principal stress directions, and their lengths (given by the eigenvalues of $\boldsymbol{\sigma}$) represent the relative magnitude of stress. Blue arrows represent contraction, and orange arrows represent expansion. (*M* and *N*) σ and θ vs. time in two-filament simulations. (*O* and *P*) Comparison of σ and $\tilde{I}_2$ in rigid and semiflexible two-filament simulations. (*Q–T*) Comparison between σ and I_2 for one time step of a two-filament simulation, with $\Delta t = 2 \times 10^{-5}$ s. To see this figure in color, go online.

motor traverses the filaments from the minus to plus ends, the filaments move and rotate such that their final position is a mirror image of the original. As reported by Lenz (9), this polarity-reversal symmetry causes the initial contraction and subsequent expansion to cancel. Principal stress arrows in the upper panel confirm this. The result is no net contraction for rigid filaments. However, the picture is different for semiflexible filaments, as the lower row (Fig. 4, *F–J*) reveals. When the motor begins to move, filament bending increases θ, increasing contraction in the x-direction. Subsequently, as the motor positions become favorable to expansion, the angle between the filaments decreases (see the *fourth image* in the *lower panel*), decreasing the magnitude of expansion. Consequently, the semiflexible filaments experience net contraction, providing evidence of the force asymmetry.

To verify this, we plot the bulk stress and θ vs. time for both rigid and semiflexible filaments. The bulk stress results in Fig. 4*K* confirm that rigid filaments experience no net contraction because the magnitude of early contraction is equal to the magnitude of later expansion. The results in Fig. 4*L* support this, in which the angle θ for the initial contraction mirrors the angle for the subsequent expansion. In contrast, for semiflexible filaments the structure experiences larger contractile than expansive stress. This is because filament bending leads to an asymmetric pattern in θ with time, with a decrease as the motor approaches the plus ends. As a result, the semiflexible filaments are unable to attain the large expansion that occurs toward the end of the rigid filament solution. This analysis confirms that a force asymmetry is a possible explanation for bending-induced actomyosin contraction.

A heuristic index predicts stress generated by two-filament-motor assemblies

Inspired by the previous results on the contraction of a two-filament-motor system, we propose a heuristic index that summarizes the contractile potential of two filaments,

$$I_2 = \left[\frac{2(m_1 + m_2)}{L_1 + L_2} - 1\right] \sin^2\left(\frac{\theta}{2}\right). \tag{8}$$

In Eq. 8, the left term in the brackets describes the length of the expansive and contractile branches, such that it is -1 if both motors are at the minus ends (contractile) and 1 if

both motors are at the plus ends (expansive). To capture the effect of angle, the term in the right brackets is zero if $\theta = 0$ and 1 if $\theta = \pi$.

To confirm the effect of angle on contraction, we plot I_2 (Eq. 8) vs. time in the two-filament simulations. In Fig. 4, *M and N*, we multiplied I_2 by a constant such that its minimum is equal to the minimal stress obtained in the simulation. We refer to this normalized index as $\tilde{I}_2$. The index accurately predicts the bulk stress in both simulations. Of particular note, $\tilde{I}_2$ correctly predicts the loss of contraction with semiflexible filaments, as Fig. 4*N* shows. Combined with Fig. 4*L*, this shows that filament bending facilitates contraction by influencing the angle between filaments, such that larger angles occur under contraction than under expansion.

To confirm the predictive ability of Eq. 8, we compute I_2 for varying m_1, m_2, and θ. For each configuration, we compute one time step and compare the simulated bulk stress with Eq. 8. The results in Fig. 4, *O–R* show that the two-filament index I_2 effectively captures the stress generated by two filaments. This is true if we hold $m_1 = m_2$ and vary θ (as in Fig. 4, *O and P*) and if we hold θ constant and vary both m_1 and m_2 (as in Fig. 4, *Q and R*).

Protein friction enables network-scale contraction

Protein friction, either from cross-linking or filament contact, penalizes relative motion where filaments overlap. Previous studies have suggested that intermediate cross-linker density maximizes contraction (25,29,32,43,68,69). Without cross-linking, filaments move independently of each other and are unable to generate collective contraction. However, strongly cross-linked networks generate large resistance to filament motion as myosin moves, which also inhibits contraction. To investigate this dependence using our model, we varied the protein friction drag coefficient, λ_{pf}, and computed 10 simulations with each parameter value. Results from these simulations are shown in Fig. 5.

Fig. 5*A* shows the relationship between λ_{pf} and bulk stress. As expected, networks become more contractile as λ_{pf} increases from 0. Although the precise value of the protein friction coefficient for actin filaments is unknown, Ward et al. (48) suggest a protein friction due to filament contact of approximately $\lambda_{pf} = 30$ pN μm^{-1} s. Estimating λ_{pf} based on the cross-linker α-actinin yields approximately $\lambda_{pf} = 20$ pN μm^{-1} s (see Supporting materials and methods). Both values are sufficient to demonstrate contractile bias. Subsequent increases in λ_{pf} beyond these values incur diminishing returns, such that contractility becomes stable after approximately $\lambda_{pf} = 200$ pN μm^{-1} s. We do not observe a U-shaped curve in stress with λ_{pf}. A possible explanation is the sparseness of our simulated networks, which does not enable sufficient connectivity to restrict contraction given that we assume no protein friction between filament pairs with a motor attached.

Plots of the time-averaged curvature and I_2 in Fig. 5, *B and C*, respectively, demonstrate that contraction correlates with increased curvature and decreased I_2. An important finding is that filament bending does not occur in the absence of protein friction. This is because protein friction supplies resistance to motion at specific points along the filament. Without this drag, neglecting thermal fluctuations, the filament will tend to adopt the energetically preferable straight configuration. Therefore, protein friction is essential to contraction. Furthermore, only a small increase in filament bending is attainable by increasing the protein friction coefficient beyond the biologically feasible value of $\lambda_{pf} = 30$ pN μm^{-1} s.

Viscous friction inhibits contraction

The viscous drag coefficient λ_a represents drag between actin filaments and structures external to the network. This can arise from drag between the filaments and the cytoplasm or drag between filaments and a dense, homogeneous background network that interacts uniformly with the simulated filaments. Increasing λ_a thus corresponds to increasing cytoplasm viscosity or increasing the network density. In vitro experiments by Murrell and Gardel (16) showed that increasing adhesion between actomyosin networks and the membrane inhibits contraction. We suggest that increased membrane adhesion corresponds to an increase in drag coefficient in our model because both restrict filament motion.

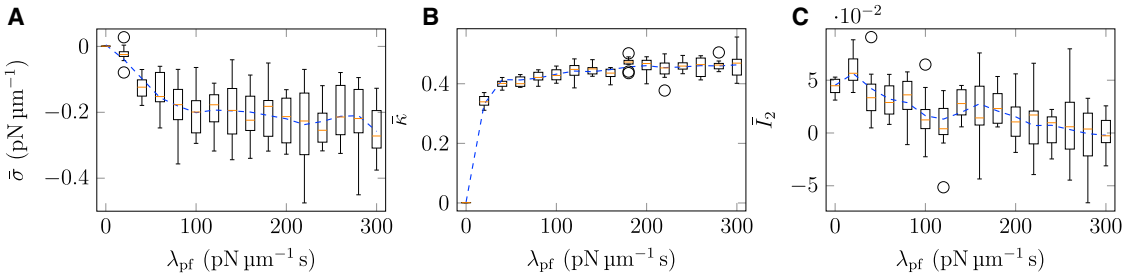

FIGURE 5 The effect of protein friction coefficient, λ_{pf}, on (*A*) $\bar{\sigma}$, (*B*) $\bar{\kappa}$, and (*C*) $\bar{I}_2$. Boxplots represent data from 10 simulations with a given parameter, and the dashed curve represents mean data smoothed with a Savitsky-Golay filter. To see this figure in color, go online.

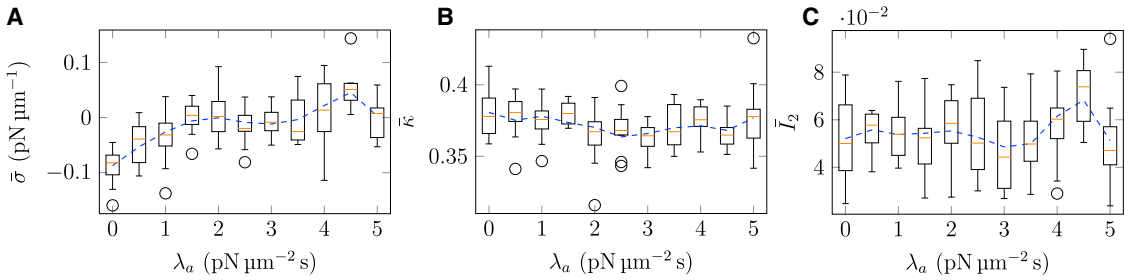

FIGURE 6 The effect of viscous drag coefficient, λ_a, on (*A*) $\overline{\sigma}$, (*B*) $\overline{\kappa}$, and (*C*) $\bar{I}_2$. Boxplots represent data from 10 simulations with a given parameter, and the dashed curve represents mean data smoothed with a Savitsky-Golay filter. To see this figure in color, go online.

For these reasons, we are interested in how contractility depends on λ_a.

We varied λ_a and performed 10 simulations for each parameter value. These results are shown in Fig. 6 *A*. As predicted by experiments, network contractility increases as we decrease λ_a. Interestingly, Fig. 6, *B and C* show that this increased contraction does not correspond to an increase in filament curvature or decrease in the two-filament index. Instead, a possible explanation is that increasing λ_a increases resistance to actin filament movement. When myosin motors exert forces on the network, a larger proportion is used to overcome drag as λ_a increases. This inhibits the ability of myosin motors to remodel the network, and this slower remodeling results in decreased contraction.

Myosin unbinding does not affect the mechanism of contraction

Myosin motor unbinding is another feature of our model that might influence contractility. In our simulations, motor unbinding is governed by Bell's law. All motors that have not reached the end of a filament unbind with a rate that depends on the spring force on the motor and the reference off rate, $k_{\text{off},m}$. To investigate how this off rate affects contractility, we computed a series of simulations with varying $k_{\text{off},m}$ and present results in Fig. 7, *A–C*.

Overall, the reference off rate has no consistent effect on stress. However, Fig. 7, *B and C* suggest that the means of contraction changes as $k_{\text{off},m}$ changes. A possible explanation is that $k_{\text{off},m}$ governs the expected time for which a motor remains attached to the filaments. For example, lower values of $k_{\text{off},m}$ enable motors to remain attached to actin filaments for longer time. Highly persistent motors have a longer time to initiate bending, and therefore, curvature increases as $k_{\text{off},m}$ decreases (see Fig. 7*B*). However, such persistent motors also walk further toward the plus ends, increasing I_2 (see Fig. 7*C*). As previously shown, motor positioning closer to the plus ends is favorable for expansion. The competing effects of filament bending and motor position enable disordered networks to generate similar contractile stress for all reference motor off rates tested.

We also tested how the force dependence introduced by Bell's law influences contractility. To do this, we performed 25 simulations with both rigid and semiflexible filaments and compared the time-averaged bulk stress results with the default simulations in Fig. 3*A*. Results with force-independent unbinding are given in Fig. 7 *D*. Compared to simulations with force-dependent unbinding, simulations with force-independent unbinding display a small bias to contraction in both rigid and semiflexible simulations. A possible explanation is that the stretching force on a myosin motor is larger for antiparallel filament pairs undergoing contraction. With force-dependent unbinding, motors more readily unbind from these antiparallel filaments, decreasing contractility. However, because the results in Fig. 7*D* are similar to Fig. 3*A*, this does not affect the mechanism of contraction.

Actin filament turnover enables persistent contraction

In biological cells, actin filament turnover is an important process that enables sustained contraction. Turnover refers to the exchange of proteins with the background cytoplasm and introduces randomness. Without turnover, actomyosin networks have been shown to lose contractility over time (7,12,17,27,43,45). To investigate whether our model replicates this behavior, we varied the actin filament turnover rate, $k_{\text{off},a}$, and present results for the simulated stress in Fig. 8*A*. Time-averaged stress results show increased contraction as we increase actin turnover rate. In support of this, Fig. 8, *B and C* show that increased actin turnover corresponds to a decrease in mean integrated filament curvature, and the two-filament index shows bias toward expansive configurations.

To investigate the time dependence of contractile stress with and without turnover, we plot the mean bulk stress in the 10 simulations versus time for $k_{\text{off,a}} = 0$ s^{-1} (no turnover) and $k_{\text{off},a} = 0.2$ s^{-1} (fast turnover). With no turnover, there is a loss of contractility as time progresses (see Fig. 8*D*), whereas no trend occurs with fast turnover. Because both networks in Fig. 8, *D and E* show similar contractile stress at $t = 0$, the results in Fig. 8*A* occur because the network loses contractility if there is no turnover, decreasing time-averaged stress $\overline{\sigma}$.

Previous studies have shown that loss of contraction in the absence of turnover is associated with pattern formation in the network. This involves filaments aggregating in asters

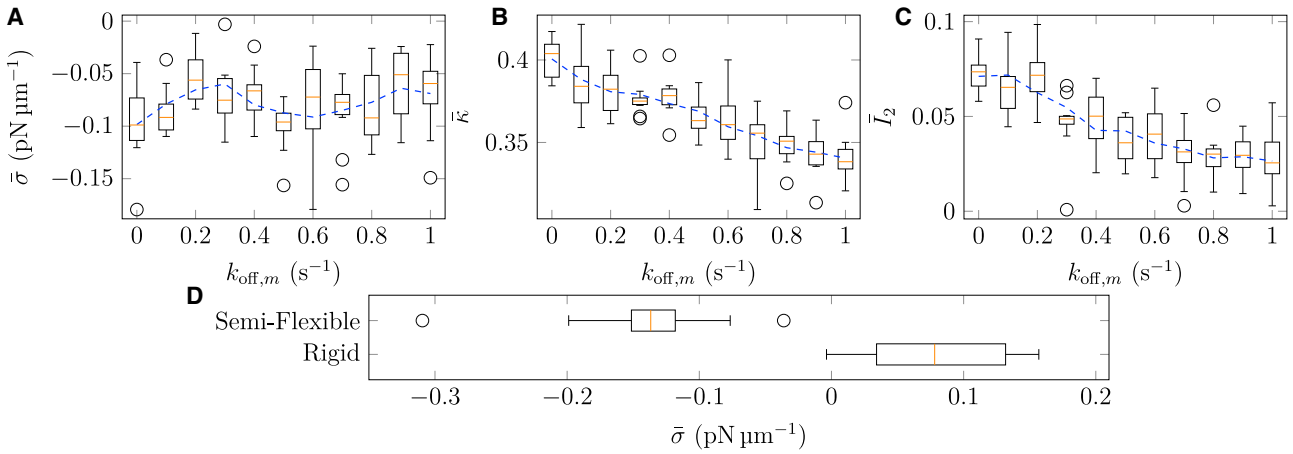

FIGURE 7 (*A–C*) The effect of reference motor off rate, $k_{\mathrm{off},m}$, on (*A*) $\bar{\sigma}$, (*B*) $\bar{\kappa}$, and (*C*) $\bar{I}_2$. Boxplots represent data from 10 simulations with a given parameter, and the dashed curve represents mean data smoothed with a Savitsky-Golay filter. (*D*) Box plots comparing mean $\bar{\sigma}$ in 25 semiflexible networks and 25 rigid networks, with force-independent motor unbinding. To see this figure in color, go online.

(71) or bundles (72), after which they do not move under molecular motor activity. To investigate whether filament aggregation occurs in our simulations, we computed the distance between all pairs of nodes on different filaments. If the distribution of these distances differs from the expected distribution for two random points in a square, we conclude that filaments have aggregated. An example comparison of these distance distributions at 300 s and the corresponding network images are provided in Fig. 8, *F–I*. With no turnover, there are two peaks in the distribution of distances that are not predicted by the theoretical distribution. In contrast, the distance distribution closely matches the theoretical distribution in the simulation with fast turnover, $k_{\mathrm{off},a} = 0.2\ \mathrm{s}^{-1}$. This provides evidence that actin filaments aggregate with no turnover. Fast turnover prevents this filament aggregation by introducing randomness to filament positions, enabling persistent contraction. Similar distributions occur across all simulations, a complete summary of which is given in the Supporting materials and methods.

Simulated networks do not exhibit periodic pulsation

Interestingly, periodic or pulsed contraction has been observed in experiments and simulations with filament turnover (17,43,73,74). Some authors have suggested that biochemical signals external to the network are responsible for this pulsation (73,74). However, recent work by Yu et al. (75) showed that pulsation might be an inherent result of actomyosin mechanics, caused by actin treadmilling or severing. As Fig. 8, *D and E* show, stress rises and falls in our simulations with or without turnover, indicating pulse-like behavior. To investigate whether solutions with turnover have a characteristic period of pulsation, we simulated 10 random networks to $T = 600$ s, with default parameters. Plotting the autocorrelation of the stress signal then enables us to determine whether a characteristic period exists. These results are shown in Fig. 8*J*. Autocorrelation compares the original stress signal and a time-delayed version and returns the correlation coefficient at a function of the time delay. If stress generation is periodic with period *T*, we would see peaks in the autocorrelation at all multiples of *T*. In Fig. 8*J*, no such peaks appear in the first 5 min of the 10 solutions and mean data. Therefore, although our results show oscillations in contractile stress, these oscillations are aperiodic.

Our findings extend the results of Belmonte, Leptin, and Nédélec (17), who used visual inspection of simulations to show that pulsation occurs in networks with turnover. Our results are consistent with observations that pulsation occurs because of biochemically regulated periodic formation of actomyosin networks (73,74) and not necessarily periodic stress generation within the networks. Observing periodic mechanical behavior would require additional features to those in our model. Examples might include actin treadmilling or severing, which Yu et al. (75) showed to be necessary for pulsed contraction in the absence of biochemical regulation.

Theoretical results provide experimentally testable predictions

Our theoretical work provides predictions that could be tested using in vitro actomyosin assays. One testable prediction is the detailed dependence of stress on filament flexural rigidity (Fig. 3*B*). This could be tested using actomyosin assays similar to Alvarado et al. (76) by comparing experimental measurements of force or contraction with our stress results. Another testable prediction is the dependence of the protein friction coefficient on stress (Fig. 5*A*). This could be tested by varying the concentration of cross-linkers, which governs λ_{pf} according to the formula in the Supporting materials and methods. Furthermore, results from in vitro assays could be compared with our

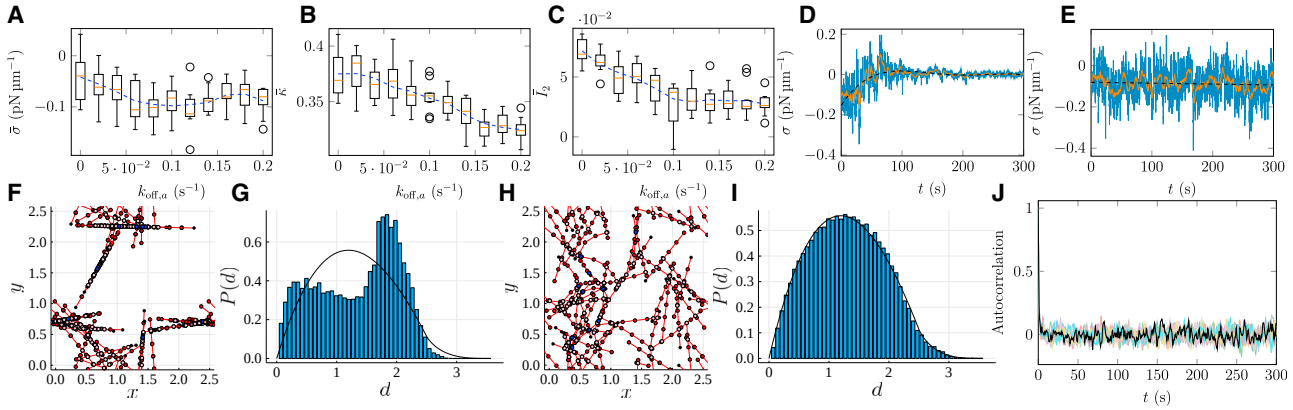

FIGURE 8 (*A–C*) The effect of actin turnover rate, $k_{\mathrm{off},a}$, on (*A*) $\bar{\sigma}$, (*B*) $\bar{\kappa}$, and (*C*) $\bar{I}_2$. Boxplots represent data from 10 simulations with a given parameter, and the dashed curve represents mean data smoothed with a Savitsky-Golay filter. (*D* and *E*) Mean bulk stress (*blue curve*) for 10 simulations versus time, with (*D*) $k_{\mathrm{off},a} = 0$ s^{-1} and (*E*) $k_{\mathrm{off},a} = 0.2$ s^{-1}. The orange curve is a moving average with window width 10 s, and the dashed curve is a fit to mean data. (*F* and *I*) Network configurations and distributions of the distances between pairs of actin filament nodes in the network at $t = 300$ s. Blue bars represent simulation results, and the black curve is the theoretical distribution for the distance between two random points in a square (70). (*F* and *G*) No turnover, $k_{\mathrm{off},a} = 0$ s^{-1}. (*H* and *I*) Fast turnover, $k_{\mathrm{off},a} = 0.2$ s^{-1}. (*J*) Autocorrelation function of the stress σ. The transparent curves represent 10 individual simulations, and the opaque black curve is the autocorrelation of the mean stress. To see this figure in color, go online.

predictions of the effect of actin filament turnover rate on stress (Fig. 8*A*). Computing a pair-correlation function to mimic the distance distributions visualized in Fig. 8, *G and I* would also enable comparison with the quantitative predictions on aggregation reported in more detail in the Supporting materials and methods. Overall, experimental validation could uncover whether the minimal mechanics included in our model is sufficient. If not, possible extensions to the model include simulating filament polymerization or treadmilling and incorporating a three-dimensional description of the material mechanics (52).

CONCLUSIONS

Contraction of disordered actomyosin networks is essential to biological cell function. Because the origins of this contraction are not yet fully understood, scientists have worked to build an inventory of possible contraction mechanisms. In this study, we investigated the hypothesis that protein friction, arising from cross-linking or solid friction between actin filaments, enables the contraction of networks consisting of semiflexible actin filaments. We achieved this by developing an agent-based mathematical model for two-dimensional actomyosin networks. By formulating the force-balance equations as a gradient flow, our model provides a way of quantifying network stress. Numerical simulations confirmed that actin filament bending facilitates a force asymmetry that biases contraction over expansion in random networks. Importantly, network-scale bending is only possible with protein friction, making protein friction crucial to contraction.

To understand the bending-induced force asymmetry at the microscopic scale, we simulated the simplest actomyosin system consisting of a single myosin motor bound to two actin filaments. For both rigid and semiflexible filaments, the contractile force depends on the motor relative positions and the angle between the two filaments. As the motor moves from the minus to the plus ends, semiflexible filaments generate a wider angle than rigid filaments. Because these wider angles are more conducive to contraction, our microscopic simulations showed that filament bending induces contractile bias at the microscopic scale. Furthermore, this confirmed that bending forces are sufficient to facilitate contraction.

Our simulations also confirmed previous experimental and theoretical results that filament turnover is required to sustain contraction. Although actin bending and protein friction facilitate contraction, without turnover the filaments aggregate and form patterns, after which the network loses contractility. In our simulations, introducing turnover causes a more random spatial distribution of filaments and enables the network to sustain contractility. However, in many cell types, actin filaments can form contractile actomyosin bundles such as stress fibers, which are aggregated structures that sustain and mediate contractility (77). An important application of our modeling and simulation framework will be to identify the minimal mechanisms that enable self-organization and persistence of such bundles, even in networks with fast turnover. We plan to tackle this problem in future work.

SUPPORTING MATERIAL

Supporting material can be found online at https://doi.org/10.1016/j.bpj.2021.08.012.

AUTHOR CONTRIBUTIONS

A.K.Y.T. and D.B.O. designed the research and developed the mathematical model. A.K.Y.T. performed the numerical simulations, analyzed the data, and wrote the manuscript, with guidance from D.B.O. and A.M.

ACKNOWLEDGMENTS

The authors acknowledge funding from the Australian Research Council Discovery Program (grant number DP180102956), awarded to D.B.O. and A.M.

REFERENCES

1. Gautel, M. 2011. The sarcomeric cytoskeleton: who picks up the strain? *Curr. Opin. Cell Biol.* 23:39–46.
2. Pollard, T. D. 2010. Mechanics of cytokinesis in eukaryotes. *Curr. Opin. Cell Biol.* 22:50–56.
3. Yamada, K. M., and M. Sixt. 2019. Mechanisms of 3D cell migration. *Nat. Rev. Mol. Cell Biol.* 20:738–752.
4. Chalut, K. J., and E. K. Paluch. 2016. The actin cortex: a bridge between cell shape and function. *Dev. Cell.* 38:571–573.
5. Pollard, T. D. 2014. The value of mechanistic biophysical information for systems-level understanding of complex biological processes such as cytokinesis. *Biophys. J.* 107:2499–2507.
6. Cheffings, T. H., N. J. Burroughs, and M. K. Balasubramanian. 2016. Actomyosin ring formation and tension generation in eukaryotic cytokinesis. *Curr. Biol.* 26:R719–R737.
7. Rubinstein, B. Y., and A. Mogilner. 2017. Myosin clusters of finite size develop contractile stress in 1D random actin arrays. *Biophys. J.* 113:937–947.
8. Gordon, D., A. Bernheim-Groswasser, …, O. Farago. 2012. Hierarchical self-organization of cytoskeletal active networks. *Phys. Biol.* 9:026005.
9. Lenz, M. 2014. Geometrical origins of contractility in disordered actomyosin networks. *Phys. Rev. X.* 4:041002.
10. Hiraiwa, T., and G. Salbreux. 2016. Role of turnover in active stress generation in a filament network. *Phys. Rev. Lett.* 116:188101.
11. Carlsson, A. E. 2006. Contractile stress generation by actomyosin gels. *Phys. Rev. E Stat. Nonlin. Soft Matter Phys.* 74:051912.
12. Oelz, D. B., B. Y. Rubinstein, and A. Mogilner. 2015. A combination of actin treadmilling and cross-linking drives contraction of random actomyosin arrays. *Biophys. J.* 109:1818–1829.
13. Kruse, K., and F. Jülicher. 2000. Actively contracting bundles of polar filaments. *Phys. Rev. Lett.* 85:1778–1781.
14. Lenz, M., M. L. Gardel, and A. R. Dinner. 2012. Requirements for contractility in disordered cytoskeletal bundles. *New J. Phys.* 14:033037.
15. Wollrab, V., J. M. Belmonte, …, G. H. Koenderink. 2018. Polarity sorting drives remodeling of actin-myosin networks. *J. Cell Sci.* 132:jcs219717.
16. Murrell, M. P., and M. L. Gardel. 2012. F-actin buckling coordinates contractility and severing in a biomimetic actomyosin cortex. *Proc. Natl. Acad. Sci. USA.* 109:20820–20825.
17. Belmonte, J. M., M. Leptin, and F. Nédélec. 2017. A theory that predicts behaviors of disordered cytoskeletal networks. *Mol. Syst. Biol.* 13:941.
18. Kamasaki, T., M. Osumi, and I. Mabuchi. 2007. Three-dimensional arrangement of F-actin in the contractile ring of fission yeast. *J. Cell Biol.* 178:765–771.
19. De La Cruz, E. M., and M. L. Gardel. 2015. Actin mechanics and fragmentation. *J. Biol. Chem.* 290:17137–17144.
20. Zumdieck, A., K. Kruse, …, F. Jülicher. 2007. Stress generation and filament turnover during actin ring constriction. *PLoS One.* 2:e696.
21. Kruse, K., J. F. Joanny, …, K. Sekimoto. 2004. Asters, vortices, and rotating spirals in active gels of polar filaments. *Phys. Rev. Lett.* 92:078101.
22. Oelz, D., and A. Mogilner. 2016. Actomyosin contraction, aggregation and traveling waves in a treadmilling actin array. *Physica D.* 318–319:70–83.
23. Nédélec, F. J., and D. Foethke. 2007. Collective Langevin dynamics of flexible cytoskeletal fibers. *New J. Phys.* 9:427.
24. Freedman, S. L., S. Banerjee, …, A. R. Dinner. 2017. A versatile framework for simulating the dynamic mechanical structure of cytoskeletal networks. *Biophys. J.* 113:448–460.
25. Popov, K., J. Komianos, and G. A. Papoian. 2016. MEDYAN: mechanochemical simulations of contraction and polarity alignment in actomyosin networks. *PLoS Comput. Biol.* 12:e1004877.
26. Mendes Pinto, I., B. Rubinstein, …, R. Li. 2012. Actin depolymerization drives actomyosin ring contraction during budding yeast cytokinesis. *Dev. Cell.* 22:1247–1260.
27. Stachowiak, M. R., C. Laplante, …, B. O'Shaughnessy. 2014. Mechanism of cytokinetic contractile ring constriction in fission yeast. *Dev. Cell.* 29:547–561.
28. Kim, T. 2015. Determinants of contractile forces generated in disorganized actomyosin bundles. *Biomech. Model. Mechanobiol.* 14:345–355.
29. Chugh, P., A. G. Clark, …, E. K. Paluch. 2017. Actin cortex architecture regulates cell surface tension. *Nat. Cell Biol.* 19:689–697.
30. Head, D. A., A. J. Levine, and F. C. MacKintosh. 2003. Distinct regimes of elastic response and deformation modes of cross-linked cytoskeletal and semiflexible polymer networks. *Phys. Rev. E Stat. Nonlin. Soft Matter Phys.* 68:061907.
31. Murrell, M., P. W. Oakes, …, M. L. Gardel. 2015. Forcing cells into shape: the mechanics of actomyosin contractility. *Nat. Rev. Mol. Cell Biol.* 16:486–498.
32. Ennomani, H., G. Letort, …, L. Blanchoin. 2016. Architecture and connectivity govern actin network contractility. *Curr. Biol.* 26:616–626.
33. Pollard, T. D., and B. O'Shaughnessy. 2019. Molecular mechanism of cytokinesis. *Annu. Rev. Biochem.* 88:661–689.
34. Lenz, M., T. Thoresen, …, A. R. Dinner. 2012. Contractile units in disordered actomyosin bundles arise from F-actin buckling. *Phys. Rev. Lett.* 108:238107.
35. Bidone, T. C., W. Jung, …, T. Kim. 2017. Morphological transformation and force generation of active cytoskeletal networks. *PLoS Comput. Biol.* 13:e1005277.
36. Tawada, K., and K. Sekimoto. 1991. Protein friction exerted by motor enzymes through a weak-binding interaction. *J. Theor. Biol.* 150:193–200.
37. Milisic, V., and D. B. Oelz. 2011. On the asymptotic regime of a model for friction mediated by transient elastic linkages. *J. Math. Pures Appl.* 96:484–501.
38. McFadden, W. M., P. M. McCall, …, E. M. Munro. 2017. Filament turnover tunes both force generation and dissipation to control long-range flows in a model actomyosin cortex. *PLoS Comput. Biol.* 13:e1005811.
39. Dasanayake, N. L., P. J. Michalski, and A. E. Carlsson. 2011. General mechanism of actomyosin contractility. *Phys. Rev. Lett.* 107:118101.
40. Bell, G. I. 1978. Models for the specific adhesion of cells to cells. *Science.* 200:618–627.
41. Salbreux, G., G. Charras, and E. Paluch. 2012. Actin cortex mechanics and cellular morphogenesis. *Trends Cell Biol.* 22:536–545.
42. Saha, A., M. Nishikawa, …, S. W. Grill. 2016. Determining physical properties of the cell cortex. *Biophys. J.* 110:1421–1429.
43. Koenderink, G. H., and E. K. Paluch. 2018. Architecture shapes contractility in actomyosin networks. *Curr. Opin. Cell Biol.* 50:79–85.
44. Kim, T., M. L. Gardel, and E. Munro. 2014. Determinants of fluidlike behavior and effective viscosity in cross-linked actin networks. *Biophys. J.* 106:526–534.
45. Mak, M., M. H. Zaman, …, T. Kim. 2016. Interplay of active processes modulates tension and drives phase transition in self-renewing, motor-driven cytoskeletal networks. *Nat. Commun.* 7:10323.
46. Bormuth, V., V. Varga, …, E. Schäffer. 2009. Protein friction limits diffusive and directed movements of kinesin motors on microtubules. *Science.* 325:870–873.

47. Yoshinaga, N., and P. Marcq. 2012. Contraction of cross-linked actomyosin bundles. *Phys. Biol.* 9:046004.

48. Ward, A., F. Hilitski, …, Z. Dogic. 2015. Solid friction between soft filaments. *Nat. Mater.* 14:583–588.

49. Lin, S., X. Han, …, L. Gu. 2017. Active stiffening of F-actin network dominated by structural transition of actin filaments into bundles. *Compos. Part B Eng.* 116:377–381.

50. Mogensen, P. K., and A. N. Risbeth. 2018. Optim: a mathematical optimization package for Julia. *J. Open Source Softw.* 3:615.

51. Poynting, J. H. 1909. On pressure perpendicular to the shear planes in finite pure shears, and on the lengthening of loaded wires when twisted. *Proc. R. Soc. Lond. A Contain. Pap. Math. Phys. Character.* 82:546–559.

52. Vahabi, M., B. E. Vos, …, F. C. MacKintosh. 2018. Normal stresses in semiflexible polymer hydrogels. *Phys. Rev. E.* 97:032418.

53. Kishino, A., and T. Yanagida. 1988. Force measurements by micromanipulation of a single actin filament by glass needles. *Nature.* 334:74–76.

54. Berg, H. C. 1993. Random Walks in Biology. Princeton University Press, Princeton, NJ.

55. Gittes, F., B. Mickey, …, J. Howard. 1993. Flexural rigidity of microtubules and actin filaments measured from thermal fluctuations in shape. *J. Cell Biol.* 120:923–934.

56. Goldmann, W. H., and G. Isenberg. 1993. Analysis of filamin and alpha-actinin binding to actin by the stopped flow method. *FEBS Lett.* 336:408–410.

57. Wachsstock, D. H., W. H. Schwartz, and T. D. Pollard. 1993. Affinity of alpha-actinin for actin determines the structure and mechanical properties of actin filament gels. *Biophys. J.* 65:205–214.

58. Liu, X., and G. H. Pollack. 2002. Mechanics of F-actin characterized with microfabricated cantilevers. *Biophys. J.* 83:2705–2715.

59. Wang, F., M. Kovacs, …, J. R. Sellers. 2003. Kinetic mechanism of non-muscle myosin IIB: functional adaptations for tension generation and maintenance. *J. Biol. Chem.* 278:27439–27448.

60. Wu, J. Q., and T. D. Pollard. 2005. Counting cytokinesis proteins globally and locally in fission yeast. *Science.* 310:310–314.

61. Ferrer, J. M., H. Lee, …, M. J. Lang. 2008. Measuring molecular rupture forces between single actin filaments and actin-binding proteins. *Proc. Natl. Acad. Sci. USA.* 105:9221–9226.

62. Reichl, E. M., Y. Ren, …, D. N. Robinson. 2008. Interactions between myosin and actin crosslinkers control cytokinesis contractility dynamics and mechanics. *Curr. Biol.* 18:471–480.

63. Thoresen, T., M. Lenz, and M. L. Gardel. 2011. Reconstitution of contractile actomyosin bundles. *Biophys. J.* 100:2698–2705.

64. Erdmann, T., and U. S. Schwarz. 2012. Stochastic force generation by small ensembles of myosin II motors. *Phys. Rev. Lett.* 108:188101.

65. Oelz, D. 2014. A viscous two-phase model for contractile actomyosin bundles. *J. Math. Biol.* 68:1653–1676.

66. Stam, S., J. Alberts, …, E. Munro. 2015. Isoforms confer characteristic force generation and mechanosensation by Myosin II filaments. *Biophys. J.* 108:1997–2006.

67. Oelz, D. B., U. Del Castillo, …, A. Mogilner. 2018. Microtubule dynamics, kinesin-1 sliding, and dynein action drive growth of cell processes. *Biophys. J.* 115:1614–1624.

68. Descovich, C. P., D. B. Cortes, …, A. S. Maddox. 2018. Cross-linkers both drive and brake cytoskeletal remodeling and furrowing in cytokinesis. *Mol. Biol. Cell.* 29:622–631.

69. Freedman, S. L., G. M. Hocky, …, A. R. Dinner. 2018. Nonequilibrium phase diagrams for actomyosin networks. *Soft Matter.* 14:7740–7747.

70. Weisstein, E. W.. Square Line Picking, MathWorld — a Wolfram Web Resource. https://mathworld.wolfram.com/SquareLinePicking.html.

71. Nédélec, F. J., T. Surrey, …, S. Leibler. 1997. Self-organization of microtubules and motors. *Nature.* 389:305–308.

72. Stachowiak, M. R., P. M. McCall, …, B. O'Shaughnessy. 2012. Self-organization of myosin II in reconstituted actomyosin bundles. *Biophys. J.* 103:1265–1274.

73. Martin, A. C., M. Kaschube, and E. F. Wieschaus. 2009. Pulsed contractions of an actin-myosin network drive apical constriction. *Nature.* 457:495–499.

74. He, L., X. Wang, …, D. J. Montell. 2010. Tissue elongation requires oscillating contractions of a basal actomyosin network. *Nat. Cell Biol.* 12:1133–1142.

75. Yu, Q., J. Li, …, T. Kim. 2018. Balance between force generation and relaxation leads to pulsed contraction of actomyosin networks. *Biophys. J.* 115:2003–2013.

76. Alvarado, J., M. Sheinman, …, G. H. Koenderink. 2013. Molecular motors robustly drive active gels to a critically connected state. *Nat. Phys.* 9:591–597.

77. Pellegrin, S., and H. Mellor. 2007. Actin stress fibres. *J. Cell Sci.* 120:3491–3499.

Biophysical Journal, Volume *120*

Supplemental information

Protein friction and filament bending facilitate contraction of disordered actomyosin networks

Alexander K.Y. Tam, Alex Mogilner, and Dietmar B. Oelz

Supporting Material: Protein Friction and Filament Bending Facilitate Contraction of Disordered Actomyosin Networks

Alexander K. Y. Tam*[1], Alex Mogilner[2], and Dietmar B. Oelz[1]

[1]School of Mathematics and Physics, The University of Queensland, St Lucia, Queensland 4072, Australia

[2]Courant Institute of Mathematical Sciences, New York University, New York, NY 10012, USA

July 27, 2021

A Mathematical Model Derivation

We develop and implement an agent-based mathematical model for two-dimensional actomyosin networks. We represent actin filaments as finite-length curves in $\mathbb{R}^2$, and to track their position introduce the variables $z_i(s(t), t) \in \mathbb{R}^2$ for $i = 1, \ldots, N_a$, where N_a is the number of semi-flexible actin filaments. These represent the physical position of the actin filament, parameterised by the arc length $s(t) \in [0, L_i]$, where L_i is the length of the i-th actin filament. We consider a simplified representation of myosin motors as dumbbells that behave like stiff linear springs. The two ends of the dumbbell represent motor 'heads' that bind to actin filaments and exert forces. To track motor head positions, we define the variables $m_{ik}(t) \in [0, L_i]$, for $k = 1, \ldots, N_m$, where N_m is the number of myosin motors. These are the positions (measured from the minus end) of the k-th myosin motor along the actin filament with index i, to which it is bound. The derivation of our model in a time-discrete context then involves constructing an energy functional that depends on the degrees of freedom z_i and m_{ik}. At each time step, the solution is given by the minimiser of this functional, and advancing in time enables us to simulate network evolution. We solve the model on a two-dimensional domain with periodic boundary conditions, such that the network evolves on the surface of a torus.

A.1 Energy Functional

We write the mathematical model in a time-discrete context in terms of an energy functional that depends on the degrees of freedom $z_i(s(t), t)$, and $m_{ik}(t)$. This functional contains

*Corresponding author: alex.tam@uq.edu.au

contributions from each mechanical feature in the model. It combines the potential energy contributions for filament bending and filament and motor spring forces, with pseudo-energy terms whose variations correspond to finite-difference approximations of the thermal, drag, protein friction, and motor forces acting on filaments. At each time step of the simulation, the network evolves to minimise this energy functional. In abstract terms, the energy functional for the network is

$$\begin{aligned} E_{\text{net}} := E_{a,\text{drag}} + E_{a,\text{bend}} + E_{a,\text{spring}} + E_{a,\text{pf}} \\ + E_{m,\text{spring}} + E_{m,a}, \end{aligned} \tag{A.1}$$

where the subscripts a and m refer to actin and myosin respectively. Below, we outline the meaning and mathematical description of each term in (A.1).

We assume that viscous drag with a background medium resists motion of the actin filaments. We then obtain the pseudo-energy contribution for actin drag,

$$E_{a,\text{drag}} = \sum_{i=1}^{N_a} \int_0^{L_i} \frac{\lambda_a}{2\Delta t} \left| z_i - \boldsymbol{F} z_i^n \right|^2 \, \mathrm{d}s_i. \tag{A.2}$$

In (A.2), λ_a is the coefficient of viscous drag for actin–background interactions, and is similar to the damping term λ in the Langevin equation. The vector z_i^n represents filament positions at the previous time step, where Δt is the time step size. To account for stretching and rotation of the domain, we multiply z_i^n by the deformation gradient tensor

$$\boldsymbol{F} = \begin{bmatrix} L_{xx}/L_{xx}^n & L_{yx}/L_{yy}^n \\ L_{xy}/L_{xx}^n & L_{yy}/L_{yy}^n \end{bmatrix}, \tag{A.3}$$

which ensures both z_i and z_i^n are represented in the current spatial co-ordinates. In network-scale simulations, this drag term represents hydrodynamic drag with the background cytoplasm. An alternative interpretation of viscous drag is to assume that the simulated network is a subset of a dense, homogeneous, cross-linked network of filaments.

Since filaments are semi-flexible, we also include the contribution of elastic potential energy due to bending. This is given by

$$E_{a,\text{bend}} = \sum_{i=1}^{N_a} \int_0^{L_i} \frac{\kappa_a}{2} \left| z_i'' \right|^2 \, \mathrm{d}s_i, \tag{A.4}$$

where κ_a is the flexural rigidity, assumed constant for all actin filaments. The third term in (A.1), $E_{a,\text{spring}}$, is the energy associated with local longitudinal extension of actin filaments.

According to Hooke's law, after summing the contributions of all filaments, it is given by

$$E_{a,\text{spring}} = \sum_{i=1}^{N_a} \int_0^{L_i} \frac{\tilde{k}_a}{2} \left(|z_i'| - 1\right)^2 \, \mathrm{d}s_i, \tag{A.5}$$

where $\tilde{k}_a = k_a \Delta s$, where Δs is the segment length used in the numerical discretisation. We assume the longitudinal stiffness, k_a, to be the same for all filaments. Note that in the context of our model we regard (A.5) as a penalising potential with large coefficient k_a in order to model actin filament inextensibility and to regard s_i as an arc-length parametrisation.

Protein friction between actin filaments also contributes to the energy functional. In our model, we represent this as a viscous drag contribution that acts point-wise at intersections between actin filaments. This viscous force can arise due to contact friction between overlapping filaments [1], or as the macroscopic effect of abundant cross-linkers that undergo turnover [2]. The pseudo-energy contribution due to protein friction is

$$E_{a,\text{pf}} = \sum_{i=1}^{N_a} \sum_{\substack{j=1 \\ j>i}}^{N_a} A_{ij} \frac{\lambda_{\text{pf}}}{2\Delta t} d\left(z_i\left(\alpha_{ij}, t\right), z_j\left(\alpha_{ji}, t\right)\right)^2, \tag{A.6}$$

where λ_{pf} is the protein friction drag coefficient. In (A.6), A_{ij} is a binary variable such that $A_{ij} = 1$ if filaments i and j intersect and no motor is bound to both filaments, and $A_{ij} = 0$ otherwise. We also define $d(z_1, z_2)$ to be the shortest physical distance between two points $z_1, z_2 \in \mathbb{R}^2$ or their periodic translations, enabling us to account for periodic boundary conditions. Finally, $\alpha_{ij} \in [0, L_i]$ is the position along filament i at which the intersection with filament j occurs, and ensures that protein friction drag is applied point-wise at these intersections.

The final two terms in (A.1) model the effects of myosin motors. In the same way as we account for F-actin inextensibility, we use the penalising potential

$$E_{m,\text{spring}} = \sum_{i=1}^{N_a} \sum_{\substack{j=1 \\ j>i}}^{N_a} \sum_{k=1}^{N_m} \theta_{ijk} \frac{k_m}{2} d\left(z_i(m_{ik}, t), z_j(m_{jk}, t)\right)^2, \tag{A.7}$$

to model myosin inextensibility. Here k_m is the myosin motor spring constant which we take as very large, and θ_{ijk} is a binary variable such that $\theta_{ijk} = 1$ if myosin motor k is attached to filaments i and j, and $\theta_{ijk} = 0$ otherwise. The final term in (A.1) describes interactions between filaments and motors. We assume that myosin obeys a linear force–velocity

relation, such that positions evolve according to

$$\frac{\mathrm{d}m_{ik}}{\mathrm{d}t} = V_m \left(1 - \frac{F_k}{F_s}\right), \tag{A.8}$$

where V_m is the load-free myosin motor velocity, F_s is the motor stall force, and $F_k = k_m[z_i(m_{ik}, t) - z_j(m_{jk}, t)] \cdot z_i'$ is the projection of the spring force through the k-th myosin motor onto the direction of the i-th filament. To reproduce (A.8) as the variation of a pseudo-energy, we introduce a linear term for the load-free velocity, and a quadratic term with the same scaling as the drag terms above for the linear velocity reduction due to motor loading. The pseudo-energy then reads

$$E_{m,a} = -\sum_{i=1}^{N_a}\sum_{k=1}^{N_m} \theta_{ik}\left[F_s\left(m_{ik} - m_{ik}^n\right) - \frac{F_s}{V_m}\frac{\left(m_{ik} - m_{ik}^n\right)^2}{2\Delta t}\right], \tag{A.9}$$

where θ_{ik} is a binary variable such that $\theta_{ik} = 1$ if motor k is attached to filament i, and $\theta_{ik} = 0$ otherwise. This completes the description of all terms in the network energy functional.

A.2 Stochastic Filament and Motor Turnover

We simulate random actin filament turnover and myosin motor unbinding. Given an off-rate k_{off}, the probability of turnover or detachment in a given time step according to an exponential distribution is

$$p_{\mathrm{off}} = 1 - \mathrm{e}^{-k_{\mathrm{off}}\Delta t}, \tag{A.10}$$

where Δt is the time step size. We assume that the turnover rate for actin filaments, $k_{\mathrm{off},a}$, is constant and the same for each filament. At each time step, we use a pseudo-random number generator to simulate whether each filament will turn over. To maintain constant filament density, we immediately replace filaments that turn over with new ones at random positions and orientations. If a filament turns over, we also assume that any myosin motor attached to the filament automatically unbinds.

In contrast, we assume that the unbinding rate for myosin motors depends on the force it experiences. According to Bell's law, the force-dependent unbinding rate is given by

$$k_m = k_{\mathrm{off},m}\mathrm{e}^{F/F_{\mathrm{ref}}}, \tag{A.11}$$

where $k_{\mathrm{off},m}$ is the reference off-rate for unloaded motors, and F_{ref} is a reference force. The force to which the k-th motor is subject is the variation of the penalising potential (A.7) and given by a Hooke's law, where motors are assumed to be linear springs with equilibrium length zero. This yields $F_k = k_m d(z_i(m_{ik}, t) - z_j(m_{jk}, t))$, where i and j are

the indices of the two filaments to which the motor attaches, such that the distance term measures the motor length. Like the actin filaments, we maintain constant myosin motor density throughout the simulation by assuming that an unbound motor is immediately replaced with a new one at a random filament intersection.

A.3 Parameters

We performed network simulations in the main text with a set of default parameters. These parameters are listed in Table A.1. Additional information on the derivation of some parameters is provided below.

Table A.1: Default parameters for actomyosin network simulations.

Parameter	Symbol	Value	Units	Source
Longitudinal stiffness (actin)	k_a	1000	$\mathrm{pN\,\mu m^{-1}}$	[3]
Longitudinal stiffness (myosin)	k_m	1000	$\mathrm{pN\,\mu m^{-1}}$	[3]
Actin filament flexural rigidity	κ_a	0.073	$\mathrm{pN\,\mu m^{2}}$	[4]
Equilibrium actin filament length	L_a	1	µm	[5–7]
Actin–cytoplasm drag coefficient	λ_a	0.05	$\mathrm{pN\,\mu m^{-2}\,s}$	[8–10]
Protein friction drag coefficient	λ_{pf}	30	$\mathrm{pN\,\mu m^{-1}\,s}$	[1]
Myosin stall force	F_s	5	pN	[11–13]
Myosin free-moving velocity	V_m	0.5	$\mathrm{\mu m\,s^{-1}}$	[11, 13, 14]
Actin filament turnover rate	$k_{\mathrm{off},a}$	0.04	$\mathrm{s^{-1}}$	[15, 16]
Myosin reference off-rate	$k_{\mathrm{off},m}$	0.35	$\mathrm{s^{-1}}$	[17, 18]
Myosin reference unbinding force	F_{ref}	12.6	pN	[19]
Number of actin filaments	N_a	50	[–]	Assumption
Number of myosin motors	N_m	10	[–]	Assumption
Domain width	L_{xx}, L_{yy}	2.5	µm	Assumption
Simulation duration	T	60	s	Assumption

Longitudinal Stiffnesses, k_a, k_m: We assume that actin filament segments and myosin motors are stiff entities, and following Stachowiak et al. [3] use $k_a = m_m = 1000\,\mathrm{pN\,\mu m^{-1}}$. Although our chosen value for k_a is smaller than the value $k_a = 34.5\,\mathrm{pN\,nm^{-1}}$ observed in experiments by Liu and Pollack [20], by inspection our choices are sufficiently large to ensure filament segments and myosin motors experience negligible extension. A lower value of k_a also accounts for the low-tension regime, where actin filaments are more compliant than when under high tension [20].

Actin Filament Length: Actin filament length depends on cell type and function, and can vary across experiments. Since our modelling follows Dasanayake, Michalski, and Carlsson [6] and Hiraiwa and Salbreux [7], we adapt estimates from these authors. Dasanayake,

Michalski, and Carlsson [6] use $L_a = 2\,\mu\text{m}$, whereas Hiraiwa and Salbreux [7] use $L_a = 0.1$–$1\,\mu\text{m}$. Experimental measurements of fission yeast by Kamasaki, Osumi, and Mabuchi [5] give $L_a = 0.6\,\mu\text{m}$, and Stachowiak et al. [3] use $L_a = 1.3\,\mu\text{m}$. Based on this data, a reasonable estimate for our model is $L_a = 1\,\mu\text{m}$. When implementing semi-flexible filaments in our numerical code, we discretise this $1\,\mu\text{m}$ length into five segments of length $0.2\,\mu\text{m}$ each. We represent rigid filaments as a single segment of length $1\,\mu\text{m}$.

Actin–background drag coefficient, λ_a: Since the actin–background drag coefficient is difficult to estimate, we assume $\lambda_a = 0.05\,\text{pN}\,\mu\text{m}^{-2}\,\text{s}$ in network simulations. This value is small enough that actin–background drag has only a minor effect on the network. For an experimental justification of this parameter, we follow Oelz et al. [9], who adapt a formula from Berg [8] to obtain

$$\lambda_a = \frac{3\pi\eta}{\log(2a/b)}, \tag{A.12}$$

where η is the viscosity of the medium (in this case the cytoplasm), a is the semi-major axis length (*i.e.* half the filament length), and b is the semi-minor axis length (*i.e.* the actin filament radius). We assume filaments have the constant length $L_a = 1\,\mu\text{m}$, and thus $a = 0.5\,\mu\text{m}$. The actin filament has a diameter of $7\,\text{nm}$ [21], such that the radius is $b = 0.0035\,\mu\text{m}$. The drag coefficient $\lambda_a = 0.05\,\text{pN}\,\text{s}\,\mu\text{m}^{-2}$ then corresponds to $\eta = 0.03\,\text{pN}\,\text{s}\,\mu\text{m}^{-2}$, which is approximately 30 times the viscosity of water.

Protein Friction Drag Coefficient, λ_{pf}: We estimate the protein friction drag coefficient using experimental work by Ward et al. [1] on sliding friction between F-actin filaments. Given a pulling velocity of $0.2\,\mu\text{m}\,\text{s}^{-1}$, they obtain a frictional force of approximately $6\,\text{pN}$, suggesting that $\lambda_{\text{pf}} = 30\,\text{pN}\,\mu\text{m}^{-1}\,\text{s}$.

Under the alternative interpretation of protein friction as the macroscopic effect of abundant, transient cross-linkers, we can estimate λ_{pf} by modifying the formula used by Oelz [22]. We then have

$$\lambda_{\text{pf}} = k_\alpha \rho_\alpha s_\alpha L_\alpha \mu_{1,0,\alpha} \tag{A.13}$$

where k_α is the spring stiffness constant of the cross-linker (α-actinin), ρ_α is the maximal cross-linker density, s_α is a saturation factor, L_α is the cross-linker length, and $\mu_{1,0} = 1/(\zeta(1+\zeta/\beta))$ is a parameter that incorporates the on-rate, β, and off-rate, ζ, of the cross-linker, as derived in Milišić and Oelz [2]. Ferrer et al. [23] give $k_\alpha = 100\,\text{pN}\,\mu\text{m}^{-1}$, and Oelz [22] estimate that $\rho_\alpha = 70\,\mu\text{m}^{-1}$ and $s_\alpha = 0.05$. The length of α-actinin is $L_\alpha = 36\,\text{nm}$ [24]. From Goldmann and Isenberg [25], we obtain an on-rate of $\beta = 1\,\text{s}^{-1}$, if we assume that the concentration of α-actinin is $1\,\mu\text{M}$. Goldmann and Isenberg [25] also claim that $\zeta = 0.44\,\text{s}^{-1}$, allowing us to compute $\mu_{1,0,\alpha} = 1.5783\,\text{s}$. Thus, $\lambda_{\text{pf}} = 19.89\,\text{pN}\,\mu\text{m}^{-1}\,\text{s}$. This

is similar in magnitude to the estimate from Ward et al. [1].

Myosin Reference Off-Rate, $k_{\text{off},m}$: Stam et al. [17], citing Wang et al. [18], state that the reference off-rate $k_{off}(0)$ for non-muscle myosin is $0.35\,\text{s}^{-1}$ (IIA) and $1.71\,\text{s}^{-1}$ (IIB). This parameter therefore depends on the isoform of the myosin, and we adopt the value for myosin-IIA.

Actin Turnover Rate, $k_{\text{off},a}$: In the cell cortex, Saha et al. [15] estimate the timescale for actin filament turnover to be approximately 25 s for *C. elegans*. Based on this, we will use a turnover rate of $k_{\text{off},a} = 0.04\,\text{s}^{-1}$ in our simulations.

B Numerical Simulations and Performance Information

This appendix contains information about the numerical algorithm, including its performance, convergence, and the effect of thermal forces.

B.1 Effect of Thermal Forces

Random filament movement due to thermal fluctuations is commonly included in mathematical models for actomyosin networks. This involves adding the thermal force term $\boldsymbol{F}_{a,\text{therm}}$ to the force balance equations,

$$\begin{aligned}\mathbf{o} = \boldsymbol{F}_{a,\text{therm}} + \boldsymbol{F}_{a,\text{drag}} - \delta E_{a,\text{bend}} - \delta E_{a,\text{spring}} + \boldsymbol{F}_{a,\text{pf}} \\ - \delta E_{m,\text{spring}} + \boldsymbol{F}_{m,a}.\end{aligned} \tag{B.1}$$

In the time-discrete formulation of (B.1) in which we represent filament k as a sequence of nodes with indices i, the thermal force term applied to each node is

$$\boldsymbol{F}^{k,i}_{a,\text{therm}} := \sqrt{\frac{2k_bT\lambda_a\bar{l}^n_{k,i}}{\Delta t}}\theta^n_{k,i}. \tag{B.2}$$

In (B.2), $k_b = 1.38 \times 10^{-5}\,\mu\text{m}\,\text{pN}\,\text{K}^{-1}$ is the Boltzmann constant, T is the temperature (assumed to be 298.15 K), $\bar{l}^n_{k,i}$ is the mean length of the two filament segments adjacent to the node i of filament k at time n (or half the length of the first or last segment for minus and plus-end nodes respectively), and $\theta^n_{k,i}$ is a random vector sampled with the standard normal distribution.

To investigate how these affect our results, we performed 25 simulations with thermal fluctuations included. Bulk stress results from these simulations are presented in the box plots in Figure B.1. These results confirm that thermal fluctuations have little effect

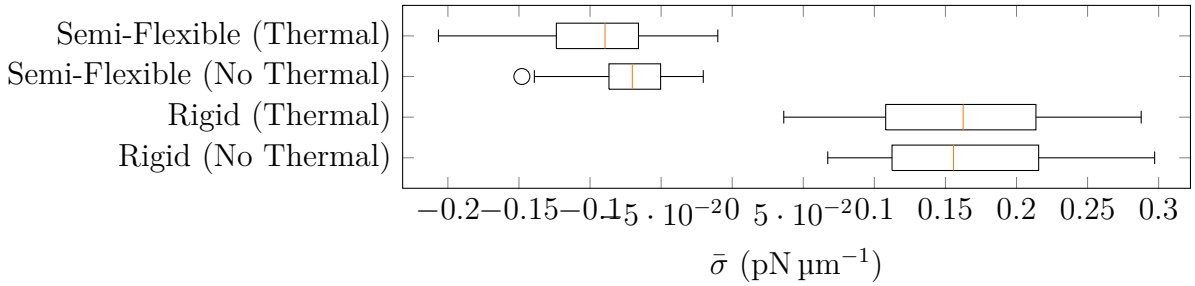

Figure B.1: Box plots comparing the bulk stress in 25 simulations of disordered networks.

on stress. Indeed, for rigid filaments their effect is negligible. In semi-flexible networks, thermal fluctuations can generate stochastic filament bending, which might cause increased contractility. However, the results presented in Figure B.1 confirm that stochastic bending effects are minor. Therefore, we omit thermal fluctuations from the main results presented in the paper, to emphasise protein friction and motor-induced bending as mechanisms of contraction.

B.2 Effect of Simulation Domain Size

Next, we performed 10 simulations on a larger (5 µm × 5 µm) domain, to confirm that the domain size and periodic boundary conditions do not affect the results. To maintain the same density of filaments and motors, for each larger simulation we used 200 filaments and 40 motors. We compare bulk stress results for these large-domain simulations with the default simulations in Figure B.2. These confirm that the domain size and periodic

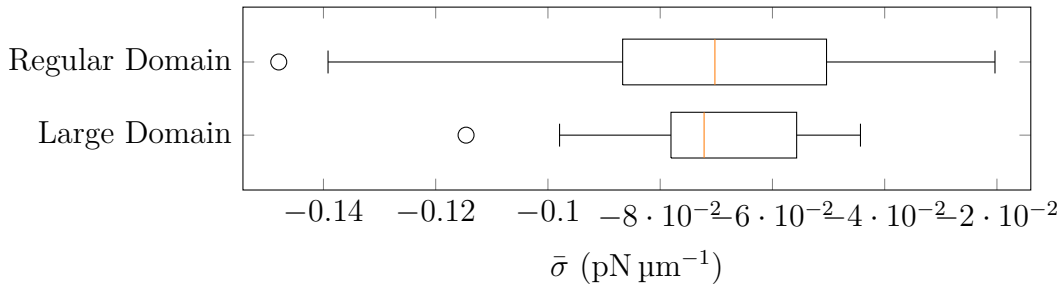

Figure B.2: Box plots comparing the bulk stress in simulations on the regular domain used throughout the manuscript, and a larger domain of size 5 µm × 5 µm.

boundary have no discernible effect on mean bulk stress $\bar{\sigma}$. Since the large-domain simulations aggregate forces for more filaments and motors than the regular-domain simulations, they exhibit variation in stress across the simulations.

B.3 Effect of System Size on Performance

The following plots describe how the simulation time and memory usage vary with the system size. In each simulation, we use the parameters from Table A.1, and compute the time and memory requirements for 100 time steps with $\Delta t = 0.05\,\mathrm{s}$. The simulations were performed using a Dell Optiplex 7060 i7-8700 desktop computer, with a 3.2GHz 6-core CPU and 15.4GB RAM, running the Linux Mint 20.1 (Cinnamon) operating system. We perform the energy minimisation using the LBFGS method from `Optim.jl`, and use `AutoDiff.jl` to evaluate the gradient.

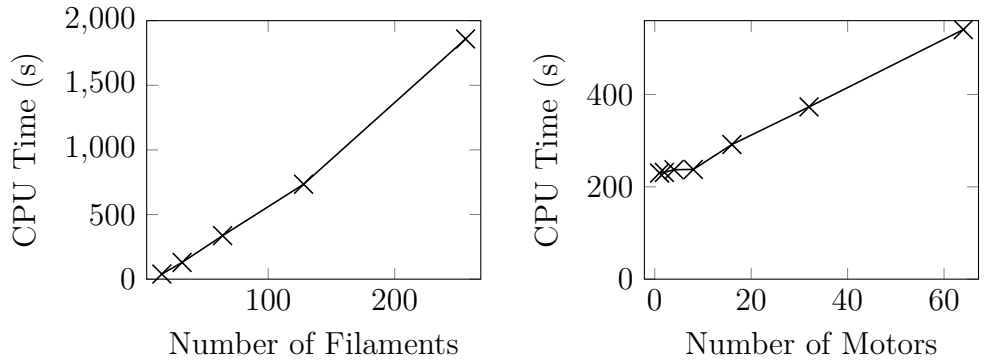

(a) Varying N_a. (b) Varying N_m.

Figure B.3: Effect of system size on simulation time. Simulations in (a) varying the number of filaments were performed using $N_m = 5$ myosin motors. Simulations in (b) varying the number of myosin motors were performed using $N_a = 50$ actin filaments.

B.4 Effect of Time Step Size on Performance

We also investigated how the time step size affects performance. In Figure B.4, we vary Δt, and measure the time to simulate a random network to $T = 5\,\mathrm{s}$. All other parameters are as in Table A.1, and the same computer was used as in §B.3. An advantage of

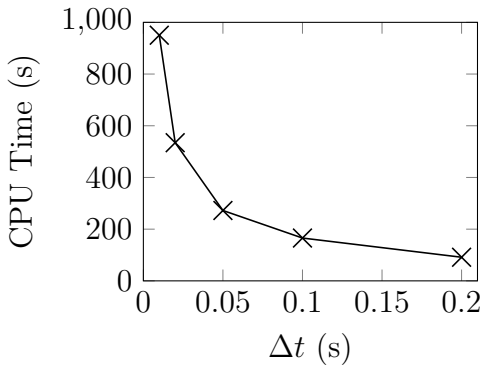

Figure B.4: Effect of time step size on simulation time.

our time-implicit numerical method is that we can take large time steps without loss of numerical stability. However, as Figure B.4 shows, the marginal performance improvement diminishes as we increase Δt. This is because the optimisation routine uses the previous time step as its initial guess. For smaller time steps, the solution will be closer to this initial guess, enabling the optimisation routine to converge faster at each step. Our results were computed with $\Delta t = 0.05\,\text{s}$, which ensured that solutions were independent of Δt.

B.5 Effect of Optimisation Routine Tolerance on Performance

The `Optim.jl` package enables users to specify the tolerance, ε, that determines when the routine considers the optimisation to have converged. Figure B.5 shows how this tolerance affects the time to simulate 101 time steps with $\Delta t = 0.05\,\text{s}$, and default parameters from Table A.1. As expected, decreasing the tolerance increases the speed of simulation. Our results were computed with $\varepsilon = 1 \times 10^{-8}$, which was sufficiently small such that solutions were independent of ε.

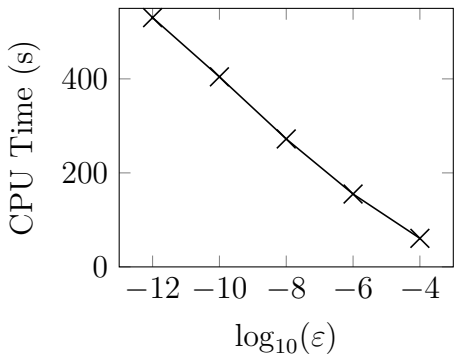

Figure B.5: Effect of optimisation routine tolerance on simulation time.

C Filament Aggregation Results

The following series of plots contains the final network configurations and distance distributions for the ten simulations performed with $T = 300\,\mathrm{s}$, and both $k_{\mathrm{off},a} = 0\,\mathrm{s}^{-1}$ and $k_{\mathrm{off},a} = 0.2\,\mathrm{s}^{-1}$.

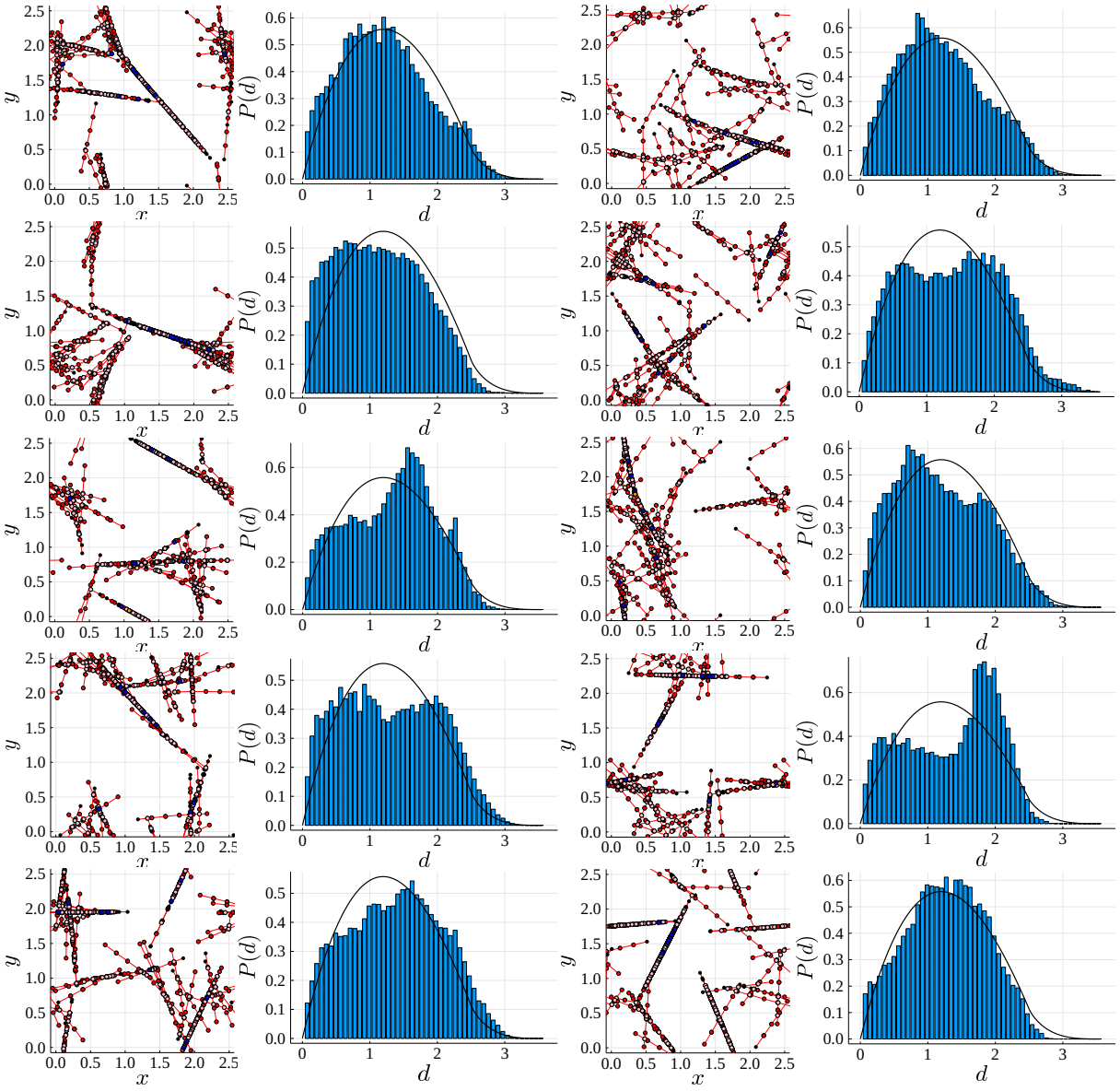

Figure C.1: Final network configurations at $t = 300\,\mathrm{s}$ and histograms of the distances between pairs of nodes on different filaments. Results presented for ten simulations with $k_{\mathrm{off},a} = 0\,\mathrm{s}^{-1}$.

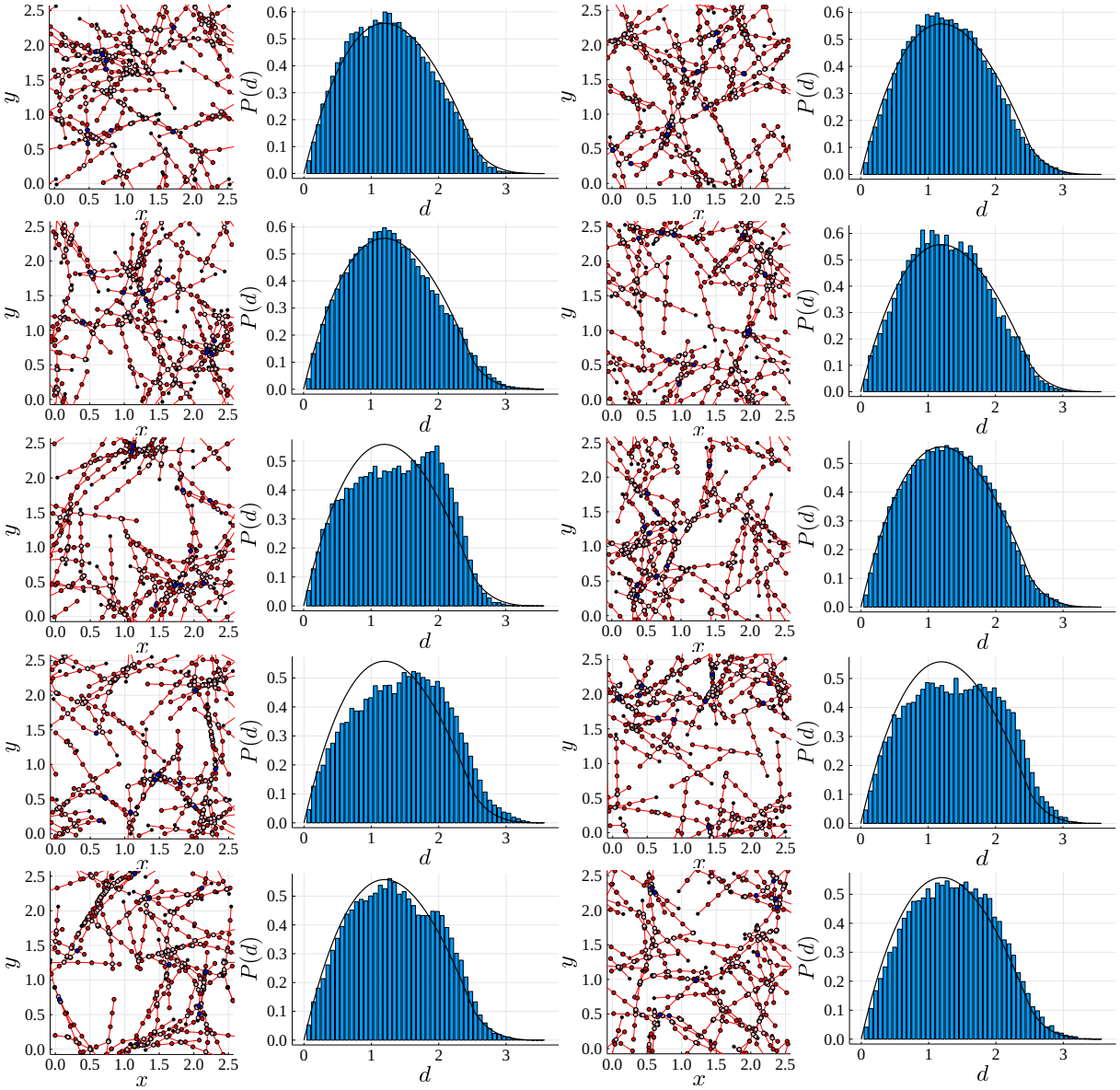

Figure C.2: Final network configurations at $t = 300\,\mathrm{s}$ and histograms of the distances between pairs of nodes on different filaments. Results presented for ten simulations with $k_{\mathrm{off},a} = 0.2\,\mathrm{s}^{-1}$.

References

[1] A. Ward, F. Hilitski, W. Schwenger, D. Welch, A. W. C. Lau, V. Vitelli, L. Mahadevan, and Z. Dogic, "Solid friction between soft filaments", *Nature Materials* 14 (2015), pp. 583–588, DOI: 10.1038/nmat4222.

[2] V. Milišić and D. B. Oelz, "On the asymptotic regime of a model for friction mediated by transient elastic linkages", *Journal de Mathématiques Pures et Appliquées* 96 (2011), pp. 484–501, DOI: 10.1016/j.matpur.2011.03.005.

[3] M. R. Stachowiak, C. Laplante, H. F. Chin, B. Guirao, E. Karatekin, T. D. Pollard, and B. O'Shaughnessy, "Mechanism of cytokinetic contractile ring constriction in fission yeast", *Developmental Cell* 29 (2014), pp. 547–561, DOI: 10.1016/j.devcel.2014.04.021.

[4] F. Gittes, B. Mickey, J. Nettleton, and J. Howard, "Flexural rigidity of microtubules and actin filaments measured from thermal fluctuations in shape", *Journal of Cell Biology* 120 (1993), pp. 923–934, DOI: 10.1083/jcb.120.4.923.

[5] T. Kamasaki, M. Osumi, and I. Mabuchi, "Three-dimensional arrangement of F-actin in the contractile ring of fission yeast", *Journal of Cell Biology* 178 (2007), pp. 765–771, DOI: 10.1083/jcb.200612018.

[6] N. L. Dasanayake, P. J. Michalski, and A. E. Carlsson, "General mechanism of actomyosin contractility", *Physical Review Letters* 107, 118101 (2011), DOI: 10.1103/PhysRevLett.107.118101.

[7] T. Hiraiwa and G. Salbreux, "Role of turnover in active stress generation in a filament network", *Physical Review Letters* 116, 188101 (2016), DOI: 10.1103/PhysRevLett.116.188101.

[8] H. C. Berg, *Random Walks in Biology*, Princeton University Press, 1993.

[9] D. B. Oelz, U. del Castillo, V. I. Gelfand, and A. Mogilner, "Microtubule dynamics, kinesin-1 sliding, and dynein action drive growth of cell processes", *Biophysical Journal* 115 (2018), pp. 1614–1624, DOI: 10.1016/j.bpj.2018.08.046.

[10] T. Kim, M. L. Gardel, and E. Munro, "Determinants of fluidlike behaviour and effective viscosity in cross-linked actin networks", *Biophysical Journal* 106 (2014), pp. 526–534, DOI: 10.1016/j.bpj.2013.12.031.

[11] D. B. Oelz, B. Y. Rubinstein, and A. Mogilner, "A combination of actin treadmilling and cross-linking drives contraction of random actomyosin arrays", *Biophysical Journal* 109 (2015), pp. 1818–1829, DOI: 10.1016/j.bpj.2015.09.013.

[12] T. Thoresen, M. Lenz, and M. L. Gardel, "Reconstitution of contractile actomyosin bundles", *Biophysical Journal* 100 (2011), pp. 2698–2705, DOI: 10.1016/j.bpj.2011.04.031.

[13] E. M. Reichl, Y. Ren, M. K. Morphew, M. Delannoy, J. C. Effler, K. D. Girard, S. Divi, P. A. Iglesias, S. C. Kuo, and D. N. Robinson, "Interactions between myosin and actin crosslinkers control cytokinesis contractility dynamics and mechanics", *Current Biology* 18 (2008), pp. 471–480, DOI: 10.1016/j.cub.2008.02.056.

[14] J. Wu and T. D. Pollard, "Counting cytokinesis proteins globally and locally in fission yeast", *Science* 310 (2005), pp. 310–314, DOI: 10.1126/science.1113230.

[15] A. Saha, M. Nishikawa, M. Behrndt, C. Heisenberg, F. Jülicher, and S. W. Grill, "Determining physical properties of the cell cortex", *Biophysical Journal* 110 (2016), pp. 1421–1429, DOI: 10.1016/j.bpj.2016.02.013.

[16] A. Zumdieck, K. Kruse, H. Bringmann, A. A. Hyman, and F. Jülicher, "Stress generation and filament turnover during actin ring constriction", *PLoS One* 2, e696 (2007), DOI: 10.1371/journal.pone.0000696.

[17] S. Stam, J. Alberts, M. L. Gardel, and E. Munro, "Isoforms confer characteristic force generation and mechanosensation by myosin II filaments", *Biophysical Journal* 108 (2015), pp. 1997–2006, DOI: 10.1016/j.bpj.2015.03.030.

[18] F. Wang, M. Kovács, A. Hu, J. Limouze, E. V. Harvey, and J. R. Sellers, "Kinetic mechanism of non-muscle myosin IIB", *Journal of Biological Chemistry* 278 (2003), pp. 27439–27448, DOI: 10.1074/jbc.M302510200.

[19] T. Erdmann and U. S. Schwarz, "Stochastic force generation by small ensembles of myosin II motors", *Physical Review Letters* 108, 188101 (2012), DOI: 10.1103/PhysRevLett.108.188101.

[20] X. Liu and G. H. Pollack, "Mechanics of F-actin characterized with microfabricated cantilevers", *Biophysical Journal* 83 (2002), pp. 2705–2715, DOI: 10.1016/S0006-3495(02)75280-6.

[21] A. Kishino and T. Yanagida, "Force measurements by micromanipulation of a single actin filament by glass needles", *Nature* 334 (1988), pp. 74–76, DOI: 10.1038/334074a0.

[22] D. B. Oelz, "A viscous two-phase model for contractile actomyosin bundles", *Journal of Mathematical Biology* 68 (2014), pp. 1653–1676, DOI: 10.1007/s00285-013-0682-6.

[23] J. M. Ferrer, H. Lee, J. Chen, B. Pelz, F. Nakamura, R. D. Kamm, and M. J. Lang, "Measuring molecular rupture forces between single actin filaments and actin-binding proteins", *Proceedings of the National Academy of Science of the United States of America* 105 (2008), pp. 9221–9226, DOI: 10.1073/pnas.0706124105.

[24] D. H. Wachsstock, W. H. Schwarz, and T. D. Pollard, "Affinity of α-actinin for actin determines the structure and mechanical properties of actin filament gels.", *Biophysical Journal* 65 (1993), pp. 205–214, DOI: 10.1016/S0006-3495(93)81059-2.

[25] W. H. Goldmann and G. Isenberg, "Analysis of filamin and α-actinin binding to actin by the stopped flow method", *Federation of European Biochemical Societies Letters* 336 (1993), pp. 408–410, DOI: 10.1016/0014-5793(93)80847-N.